J. Pineal Res. 2015; 58:397–417
Doi:10.1111/jpi.12224

Journal of Pineal Research

Journal of Pineal Research
Molecular, Biological, Physiological and Clinical Aspects of Melatonin

Anatomical and cellular localization of melatonin MT_1 and MT_2 receptors in the adult rat brain

Abstract: The involvement of melatonin in mammalian brain pathophysiology has received growing interest, but information about the anatomical distribution of its two G-protein-coupled receptors, MT_1 and MT_2, remains elusive. In this study, using specific antibodies, we examined the precise distribution of both melatonin receptors immunoreactivity across the adult rat brain using light, confocal, and electron microscopy. Our results demonstrate a selective MT_1 and MT_2 localization on neuronal cell bodies and dendrites in numerous regions of the rat telencephalon, diencephalon, and mesencephalon. Confocal and ultrastructural examination confirmed the somatodendritic nature of MT_1 and MT_2 receptors, both being localized on neuronal membranes. Overall, striking differences were observed in the anatomical distribution pattern of MT_1 and MT_2 proteins, and the labeling often appeared complementary in regions displaying both receptors. Somadendrites labeled for MT_1 were observed for instance in the retrosplenial cortex, the dentate gyrus of the hippocampus, the islands of Calleja, the medial habenula, the suprachiasmatic nucleus, the superior colliculus, the substantia nigra *pars compacta*, the dorsal raphe nucleus, and the pars tuberalis of the pituitary gland. Somadendrites endowed with MT_2 receptors were mostly observed in the CA3 field of the hippocampus, the reticular thalamic nucleus, the supraoptic nucleus, the inferior colliculus, the substantia nigra *pars reticulata*, and the ventrolateral periaqueductal gray. Together, these data provide the first detailed neurocytological mapping of melatonin receptors in the adult rat brain, an essential prerequisite for a better understanding of melatonin distinct receptor function and neurophysiology.

Baptiste Lacoste[1], Debora Angeloni[2,*], Sergio Dominguez-Lopez[1,3,*], Sara Calderoni[4], Alessandro Mauro[4,5], Franco Fraschini[6], Laurent Descarries[3,†] and Gabriella Gobbi[1]

[1]Neurobiological Psychiatry Unit, Department of Psychiatry, McGill University Health Center, McGill University, Montreal, QC, Canada; [2]Institute of Life Sciences, Scuola Superiore Sant'Anna, Pisa, Italy; [3]Departments of Pathology and Cell Biology and of Physiology, Groupe de recherche sur le système nerveux central, Université de Montréal, Montreal, QC, Canada; [4]Laboratory of Clinical Neurobiology, IRCCS Istituto Auxologico Italiano, Piancavallo, Italy; [5]Department of Neuroscience, University of Turin, Turin, Italy; [6]Department of Pharmacology, Chemotherapy and Medical Toxicology, University of Milan, Milan, Italy

Key words: brain, immunohistochemistry, melatonin receptors, neuroanatomy, rat

Address reprint requests to Gabriella Gobbi, Neurobiological Psychiatry Unit, Department Psychiatry, McGill University, 1033, Ave des Pins Ouest (room 220), Montreal, QC H3A 1A1, Canada.
E-mail: gabriella.gobbi@mcgill.ca
*These authors contributed equally to this study.
†The authors dedicate this article to the memory of Pr. Laurent DESCARRIES (1939–2012).

Received January 10, 2015;
Accepted February 26, 2015.

Introduction

Melatonin (*N*-acetyl-5-methoxytryptamine) is a neurohormone produced and released by the pineal gland and circulating in the cerebrospinal fluid (CSF) [1]. Melatonin is implicated in several neurophysiological function including circadian and seasonal rhythms, sleep, mood regulation [2], and possesses anti-inflammatory and antioxidant properties at nonphysiological doses [3–5]. The physiological actions of melatonin in brain are mediated by stimulation of two high-affinity G-protein-coupled receptors, respectively, MT_1 (also known as MTR1A or Mel-1a) and MT_2 (also known as MTR1B or Mel-1b) [6, 7].

Despite a growing attention to the involvement of melatonin in cerebral pathophysiology [8–10], information about the anatomical distribution of MT_1 and MT_2 receptors in the mammalian brain is scant. Binding sites for 2-[^{125}I]iodomelatonin have been extensively mapped in the CNS of rodents, monkeys, and humans [11–13]. In situ hybridization and RT-PCR studies in rodents have identified expression sites for melatonin receptors mRNAs in the hippocampus [14] and the hypothalamus [15–17]. In human postmortem tissue, MT_1 receptors have been observed for instance on cellular populations of the retina [18] and MT_2 receptor on pyramidal cells within subfields of the hippocampus [19].

Recently, we have reported part that MT_2 receptors are localized at somatodendritic level in rat brain regions implicated in nonrapid eye movement (NREM) sleep [10].

The present study aims at characterizing the differential anatomical distribution of both melatonin receptor proteins across the adult rat brain using both light and electron microscopic immunohistochemistry, with selective antibodies raised in one of our laboratories against both the human MT_1 and MT_2 proteins [20]. We have thus provided the first and long-awaited neuroanatomical mapping of membrane melatonin receptors proteins in the rat brain, at the cellular and subcellular levels, an essential prerequi-

site for a better understanding of melatonin receptor functions in mammals.

Material and methods

Animals

Adult male Sprague–Dawley rats (body weight: 225–250 g; n = 15) were purchased from Charles River (St Constant, QC, Canada). Housing was at constant temperature (21°C) and humidity (60%), under a fixed 12-hr light/dark cycle and with free access to food and water. All experimental procedures were conducted in accordance with the guidelines of the Canadian Council on Animal Care, and the protocols were approved by the Animal Care Committee at McGill University and Université de Montréal.

Antibodies and reagents

Polyclonal anti-MT_1 and anti-MT_2 antibodies used in the present immunohistochemical study were produced in our laboratory as described previously [20]. Subsequently, anti-MT2 antiserum was affinity purified (Primm, Milan, Italy). The sequences of the immunogenic peptides used to generated MT_1 and MT_2 antisera are shown in Fig. 1(A). Alignments between the human and rat MT_1 and MT_2 amino acid sequences are illustrated in Fig. 1(B) (BLASTP suite at http://www.ncbi.nlm.nih.gov/). The antisera were tested using a combination of immunological and functional assays. Antisera were first tested by immunocytochemistry on NIH3T3 cells transfected with either MT_1 or MT_2 cDNAs, with all due controls [20]. The transfected cells were also functionally tested with iodomelatonin radioligand binding assays [21, 22]. Subsequent work [19] and ours showed that, in Western blotting (WB) assays, antisera detected a band of the expected size (~40 kDa). For both antisera, competition assays with specific peptides prevented appearance of the bands, suggesting a high specificity. In this study, controls included WB of rat cortex, thalamus, and hypothalamus extracts (n = 3), omission of anti-MT_1 or anti-MT_2 primary antibodies (n = 2) and preincubation of primary antibodies with a 100-fold excess of their corresponding immunogenic peptide (n = 2) (Fig. 1). In Western blots of rat brain regions, the antibodies reacted with a band of ~40 kDa, corresponding to the predicted molecular weight of the native receptor proteins. For both receptors, incubation of WB membranes with pre-immune sera (PIS) prevented appearance of the bands (Fig. 1C), further demonstrating specificity. Noteworthy, in a previously published immunohistochemical study on rat brain tissue, we also reported a selective neuronal labeling using the same anti-MT_2 primary antibody and associated specificity controls [10]. In preliminary experiments on brain tissue from wild-type, MT_1 KO and MT_2 KO mice, perfusion-fixed and processed for immunohistochemistry, only ubiquitous, nonspecific staining of neurons and glial cells was observed (results not shown), precluding the use of these antibodies on mouse tissue.

The other antibodies were as follows: guinea pig antiglial fibrillary acidic protein (GFAP; Synaptic Systems, Goettingen, Germany), guinea pig antineuronal nuclei (NeuN; Millipore Chemicon, Billerica, MA, USA), and rat anticluster of differentiation molecule 11b (CD11b; Serotec, Raleigh, NC, Canada). Secondary antibodies used for light and electron microscopic immunohistochemistry were either biotinylated goat anti-rabbit IgGs (Jackson Immunoresearch, West Grove, PA, USA) or donkey anti-rabbit IgGs conjugated to 0.8-nm colloidal gold particles (Aurion, Wageningen, the Netherlands) to be revealed, respectively, with the 3,3′-diaminobenzidine (DAB) substrate kit from Vector Labs (Burlingame, CA, USA) or the HQ Silver enhancement kit from Nanoprobes

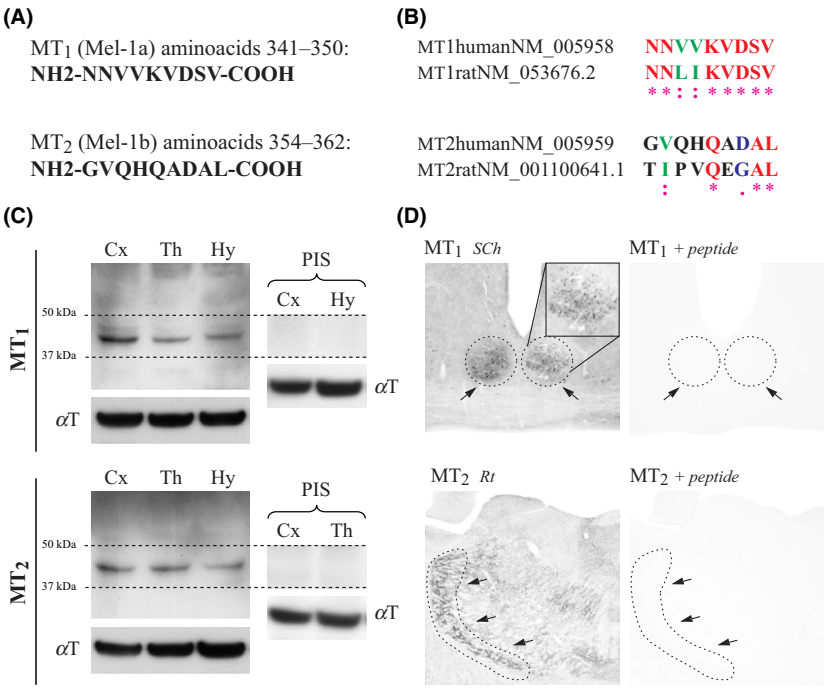

Fig. 1. Antibody specificity controls. (A) Sequences of the immunogenic peptides used to generate MT_1 and MT_2 antisera. (B) Alignments between the human and rat MT_1 and MT_2 amino acid sequences. (C) Immunoblotting with anti-MT_1 (1:5000), anti-MT_2 (1:1000) and pre-immune sera (PIS; 1:1000), and anti-alpha tubulin (αT; 1:10,000) antibodies on 30 μg of proteins loaded per lane. Cx: suprahippocampal cortex, Th: thalamus, Hy: hypothalamus. MT_1 and MT_2 receptors decorated bands of approximately 40 kDa, at their expected molecular weight. (D) As illustrated in positive control brain regions, pre-adsorption of primary antibodies with their respective immunogenic peptide completely prevented any immunostaining SCh: suprachiasmatic nucleus, Rt: reticular thalamic nucleus (designated by arrows).

(Yaphank, NY, USA). Species-specific IgGs conjugated to Alexa Fluor488 or Alexa Fluor594 (Invitrogen Corporation, Grand Island, NY, USA) were used for double immunofluorescence and confocal microscopy.

Western blotting

Immunoblotting from homogenized suprahippocampal cortex and thalamus was processed as described previously [20]. In brief, extracts were protein assayed, loaded (30 μg) in 4–12% Novex SDS-polyacrylamide gels (Life Technologies, Carlsbad, CA, USA), separated by electrophoresis, and transferred to nitrocellulose membranes which were then incubated (1 hr, RT) in a blocking buffer containing 5% nonfat milk in 0.1 M PBS and subsequently with rabbit anti-MT_1 or anti-MT_2 antibodies (overnight, 4°C), diluted, respectively, 1:5000 and 1:1000 in 5% nonfat milk in 0.1 M phosphate-buffered saline (PBS: 0.9% NaCl in 50 mM PB, pH 7.4) containing 0.15 mM NaCl and 0.1% Tween-20 (Sigma, St. Louis, MO, USA)). Membranes were further incubated (1 hr, RT) with horseradish peroxidase-conjugated secondary (anti-rabbit) antibodies (1:150,000). Loading controls were performed with mouse anti-alpha tubulin diluted 1:10,000 (overnight, 4°C), followed by anti-mouse horseradish peroxidase-conjugated secondary antibodies (1:150,000), 1 hr, RT. Immunoreactive bands, visualized by chemiluminescence (SuperSignal West Femto Chemiluminescent Substrate; Thermo Fisher Scientific, Rockford, IL, USA), were analyzed with a phosphorImager (Scanner STORM 860; GE Health Care, Piscataway, NJ, USA).

Immunohistochemistry

Animals (n = 12) were deeply anesthetized with sodium pentobarbital (80 mg/kg, i.p.) and were perfused through the heart with 250 ml of a fixative solution, followed by 500 mL of 4% paraformaldehyde (PFA) in 0.1 mM phosphate buffer (PB). To avoid the possible influence of the light/dark cycle on melatonin receptors immunolabeling and subcellular localization, all animals were sacrificed in standard condition at the same time of day (anesthesia, perfusion, and dissection always taking place between 10:00 and 11:00 am). For light (n = 9) and confocal (n = 3) microscopy, the fixative solution consisted in 0.5% acrolein in 4% PFA prepared in 0.1 mM PB, pH 7.4. For electron microscopy (n = 3), the fixation protocol was modified to improve the ultrastructural tissue preservation (2% acrolein in 1% PFA prepared in 0.2 mM PB), following earlier immunoelectron studies of G-protein-coupled receptors in brain [23, 24]. The brain and pituitary gland were carefully removed, postfixed in 4% PFA (60 min, 4°C), and washed in PBS. Fifty micrometer-thick coronal brain sections were cut with a vibratome and processed free-floating. Pituitary glands were further cryoprotected in 30% sucrose overnight at 4°C and embedded in optimal cutting temperature compound at −80°C. Twenty micrometer-thick tangential sections were then obtained using a cryostat and processed on gelatin-coated microscope slides.

For single immunoperoxidase labeling and light microscopy, sections were immersed (20 min) in 3% hydrogen peroxide (H_2O_2), rinsed in PBS, immersed (20 min) in 0.1% sodium borohydride in PBS, rinsed in PBS, and preincubated (2 hr) in a blocking solution (BS) of PBS containing 10% normal goat serum (Vector Labs), 0.5% gelatin, and 0.3% Triton X-100. Sections were then washed in PBS, incubated overnight at RT with anti-MT_1 (1:1000 in BS) or anti-MT_2 (1:250) antibody, rinsed in PBS, incubated (2 hr) with biotinylated goat anti-rabbit IgGs (1:1000), rinsed in PBS and incubated (1 hr) in a 1:1000 dilution of horseradish peroxidase-conjugated streptavidin (Jackson Immunoresearch). After washes in PBS, labeling was revealed (2–5 min) with the DAB reagent kit. This reaction was stopped in distilled water followed by washes in PB. Sections were air-dried on slides, dehydrated in ethanol, cleared in toluene, and coverslipped with DPX (Fluka, Oakville, ON, Canada). Photomicrographs were taken at low (1.6× objective), medium (6.3× objective), and high (10× objective) magnifications with a Leitz Diaplan optical microscope coupled to an Olympus DP21 color digital camera and software (Olympus Corporation, Tokyo, Japan). These images were adjusted for brightness and contrast using Adobe Photoshop (San Jose, CA, USA).

For single immunogold labeling and electron microscopy, Triton X-100 was omitted from the BS. Incubation with anti-MT_1 (1:500) or MT_2 (1:200) primary antibodies (36 hr, RT) was followed by rinses in PBS and incubation overnight at RT in a 1:50 dilution of gold-labeled, anti-rabbit donkey IgGs. After washes in PBS and sodium acetate, the size of immunogold particles was silver-enhanced (1.5 min), and the sections processed for electron microscopy as previously described [25]. In brief, sections were osmicated, dehydrated, and flat-embedded in Durcupan resin (Sigma) between two sheets of Aclar plastic (EMS, Hatfield, PA, USA). Following polymerization (48 hr, 60°C), areas of interest were excised from the Aclar sheets and glued at the tip of resin blocks. Ultrathin sections were then cut from the block surface, collected on copper grids, stained with Reynold's lead citrate, and examined under an CM100 electron microscope (Philips; Philips Electronique, St. Laurent, QC, Canada) equipped with a digital camera. Digital images were adjusted for brightness and contrast with the Adobe Photoshop software.

For double immunofluorescence and confocal microscopy, sections were preincubated 2 hr in BS, then overnight (RT) with a mixture of anti-MT_1 (1:1000) or anti-MT_2 (1:250) antibodies and either anti-NeuN (1:1000), anti-GFAP (1:500), or anti-CD11b (1:300) antibodies. After washes in PBS, sections were further incubated for 3 hr with a mix of species-specific Alexa Fluor 488- and 594-conjugated IgGs (1:200 in BS). After rinses in 0.1 M PB and distilled water, sections were mounted in Vectashield medium for fluorescence (Vector Labs) and observed with under a Zeiss LSM510 confocal microscope (Carl Zeiss, Thornwood, NY, USA), using sequential laser analysis. Images of 1024 × 1024 pixels were produced with the Zeiss LSM image browser (v4.2.0) and framed in Adobe Photoshop.

Results

In WB of adult rat brain extracts (suprahippocampal cortex, thalamus, and hypothalamus, Fig. 1C), MT_1 and

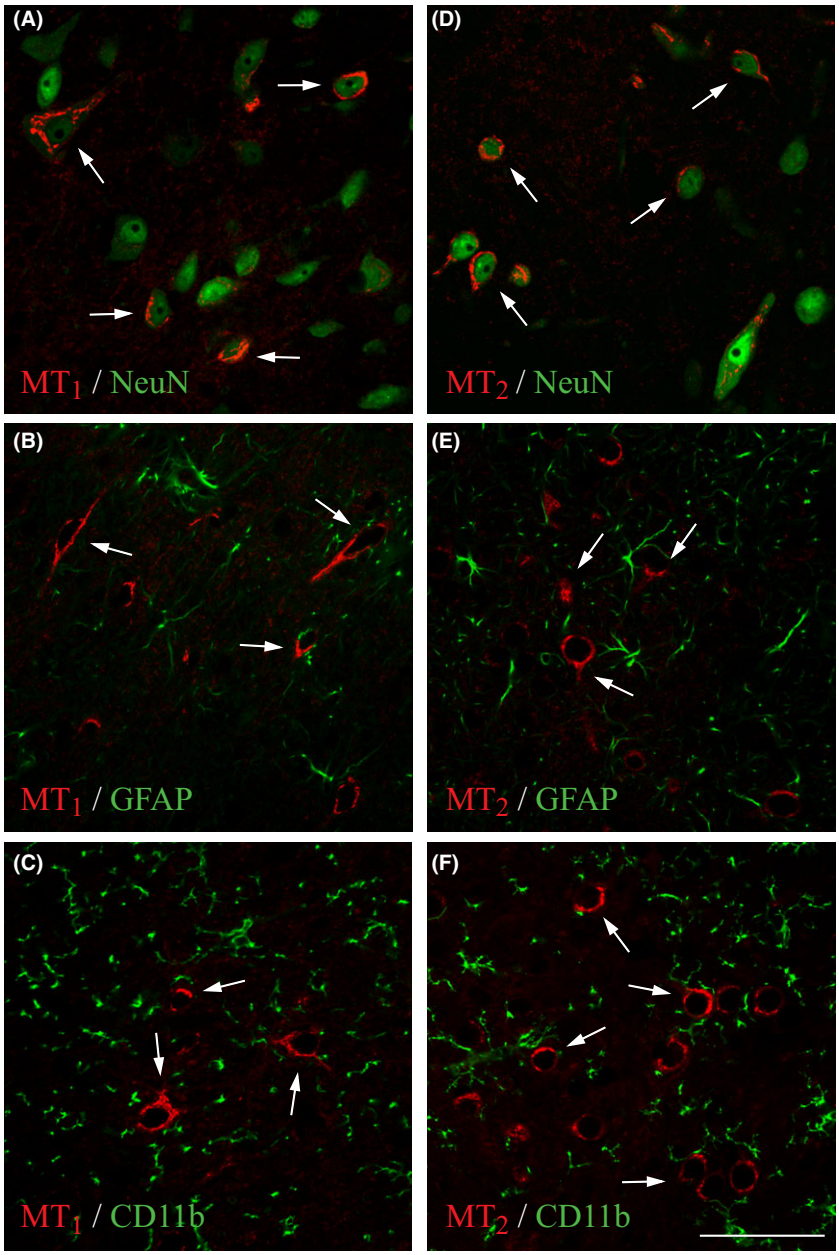

Fig. 2. Phenotype of MT_1- and MT_2-positive rat brain cells. (A–C) MT_1 receptor immunofluorescence (red) in the basal forebrain. (D–F) MT_2 receptor immunofluorescence (red) in the substantia nigra. Double immunofluorescence with the neuronal marker NeuN (A, D; green), the astroglial marker GFAP (B, E; green), and the microglial marker CD11b (C, F; green) confirmed the exclusive neuronal phenotype (arrows) of rat brain cells endowed with melatonin receptors. Scale bar: 50 μm.

MT_2 antibodies stained a band of ~40 kDa, corresponding to the predicted molecular weight of the native receptor proteins (Compute pI/Mw tool at http://web.expasy.org/compute_pi/). Incubation of membranes with the pre-immune serum (PIS) resulted in the absence of blotting signal (Fig. 1C). On brain sections from positive control regions (MT_1: suprachiasmatic nucleus, SCh; MT_2: reticular thalamic nucleus, Rt), pre-adsorption of the primary antibodies with their respective immunogenic (blocking) peptide completely prevented any immunostaining (Fig. 1D), as did omission of the primary antibodies (result not shown).

Overall, immuno-peroxidase and immuno-fluorescent stainings examined by light and confocal microscopy (Figs 2–11) revealed a selective immunoreactivity of neuronal cell bodies and dendrites in numerous brain regions (see Table 1). Using double immunofluorescence, as illustrated in Fig. 2 for the basal forebrain (MT_1) and substantia nigra (MT_2), we confirmed the neuronal phenotype of MT_1- and MT_2-positive brains cells. Both MT_1 and MT_2 labelings colocalized with the neuronal marker NeuN (Fig. 2A,D), but not with the typical astroglial (GFAP) and microglial (CD11b) markers (Fig. 2B–F). Overall (Figs 3–11), striking differences were observed in the overall localization pattern and density of MT_1 and MT_2 receptors. In regions immunoreactive for both receptors (e.g. hippocampus), the labeling appeared often complementary. MT_1 and MT_2 immunostaining was absent from several gray matter structures (e.g. lateral habenula) but strong in others (e.g. substantia nigra). Melatonin receptor immunoreactivity was absent from all white matter and brain vasculature.

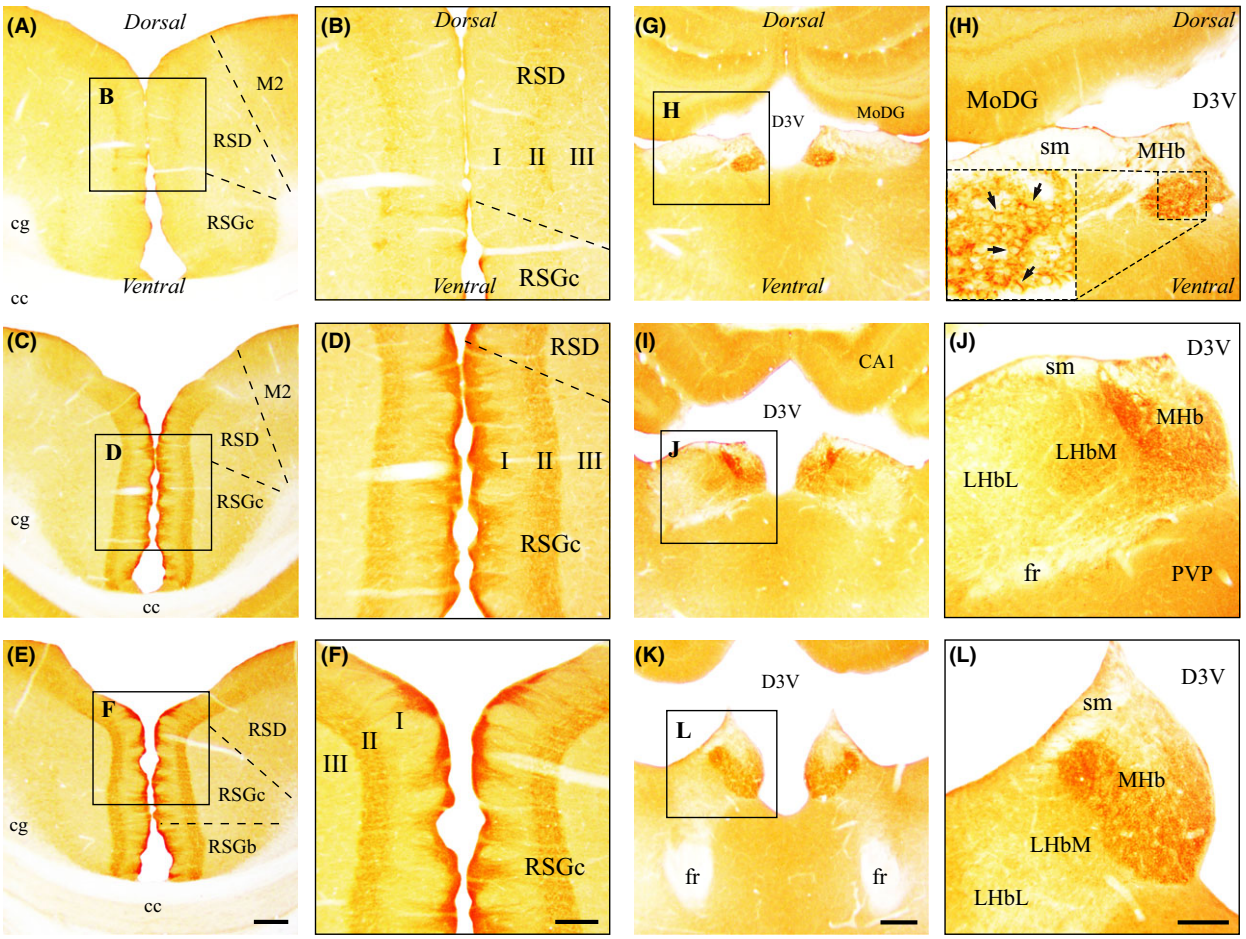

Fig. 3. Anatomical regions exclusively immunoreactive for the MT_1 receptor. (A–F) rostral (A, B), middle (C, D), and caudal (E, F) thirds of the anterior half of the retrosplenial cortex. As indicated by inserts, high magnifications of A, C, and E are, respectively, shown in B, D, and F. Stereotaxic coordinates are bregma −1.72 mm, interaural 7.28 mm (A, B); bregma −2.92 mm, interaural 6.08 mm (C, D); bregma −4.20 mm, interaural 4.80 mm (E, F). (G–L) rostral (G, H), middle (I, J), and caudal (K, L) thirds of the habenular complex. High magnifications of G, I, and K are shown, respectively, in H, J, and L. Stereotaxic coordinates are bregma −2.64 mm, interaural 6.36 mm (G, H); bregma −3.36 mm, interaural 5.64 mm (I, J); bregma −3.96 mm, interaural 5.04 mm (K, L). Dashed inserts in H illustrate a higher magnification of the medial habenula where MT_1-positive neurons appeared with a typical membrane labeling (arrows). See main list for abbreviations. Scale bars: 250 μm in E, K; 125 μm in F, L.

Cerebral cortex

Neurons endowed with MT_1 or MT_2 receptors were observed in various subdivisions of the cerebral cortex, with a generally sparse MT_2 immunostaining and a higher density for MT_1 labeling (examples in Table 1). MT_1-positive neurons were mostly found in layers II/III and V, and MT_2-positive neurons in deeper layers (V and VI) of immunoreactive cortical regions. Medially, MT_1 immunoreactivity was weak to moderate in the prefrontal (infralimbic, prelimbic, and cingulated) and frontal (secondary motor) cortices, but appeared moderate to strong in the dysgranular (RSD) and granular (RSG) retrosplenial cortices (Fig. 3A–F and Table 1), in which MT_2 immunoreactivity was faint. MT_2 immunolabeling was also barely detectable in the medial prefrontal cortex. In RSG, MT_1 immunoreactivity reached its maximal density above the dorsal hippocampus (Fig. 3E,F), then decreased rostrally and caudally. MT_1 labeling in RSG was restricted to pyramidal layer II with dendrites ascending toward the pial surface and organized in discrete bundles in layer I (Fig. 3D,F). Laterally, weak to moderate MT_1 and MT_2 immunostaining was found in the frontal (primary motor and area 3), parietal (somatosensory), and agranular insular cortices. Unlike MT_2, which yielded a weak immunostaining in both entorhinal and piriform cortices, MT_1 was almost absent from these regions. Weak MT_1 and MT_2 immunoreactivity could be detected in the claustrum and the endopiriform nucleus. Finally, almost exclusively, weak MT_1 labeling was observed in the occipital (visual) and temporal (auditory) cortices (examples in Table 1).

Basal forebrain

Rostrally, within the olfactory tubercle, ventral to the nucleus accumbens, strong MT_1 labeling density was clearly discernible in the islands of Calleja (ICj; Fig. 4A, D), regions in which MT_2 immunoreactivity was only weak (see also Table 1). MT_1 and MT_2 labeling density was comparably moderate in the ventral pallidum (VP),

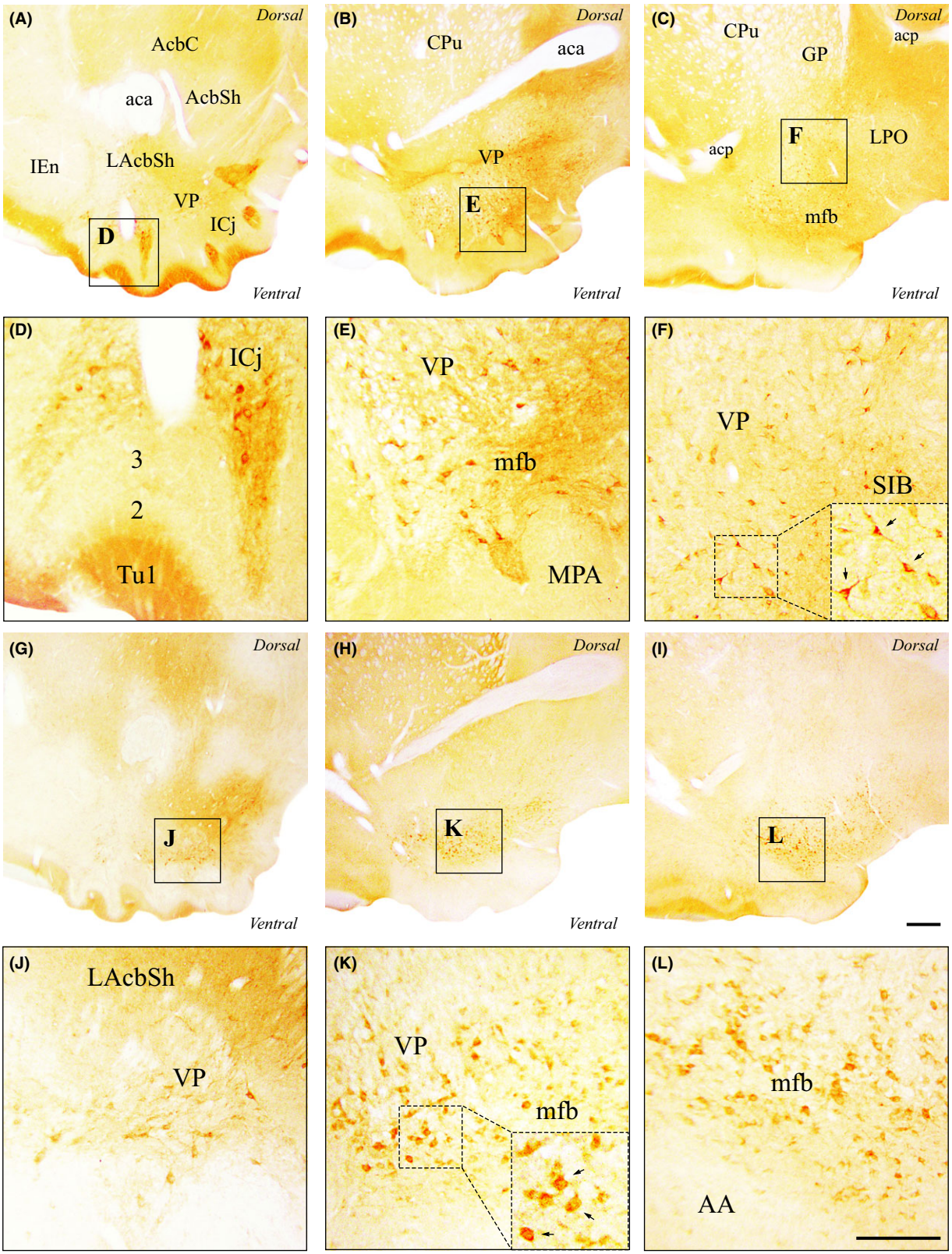

Fig. 4. Immunohistochemical localization of MT_1 and MT_2 receptors in the basal forebrain. (A–F) MT_1 immunoreactivity in the rostral (A, D), middle (B, E), and caudal (C, F) thirds of the basal forebrain. As indicated by inserts, high magnifications of A, B, and C are shown, respectively, in D, E, and F. (G–L) MT_2 immunoreactivity in the rostral (G, J), middle (H, K), and caudal (I, L) thirds of the basal forebrain. High magnifications of G, H, and I are shown, respectively, in J, K, and L. Stereotaxic coordinates are bregma 2.16 mm, interaural 11.16 mm (A, D, G, J); bregma 0.00 mm, interaural 9.00 mm (B, E, H, K); bregma −0.48 mm, interaural 8.52 mm (C, F, I, L). See main list for abbreviations. Scale bars: 250 μm in I; 125 μm in L.

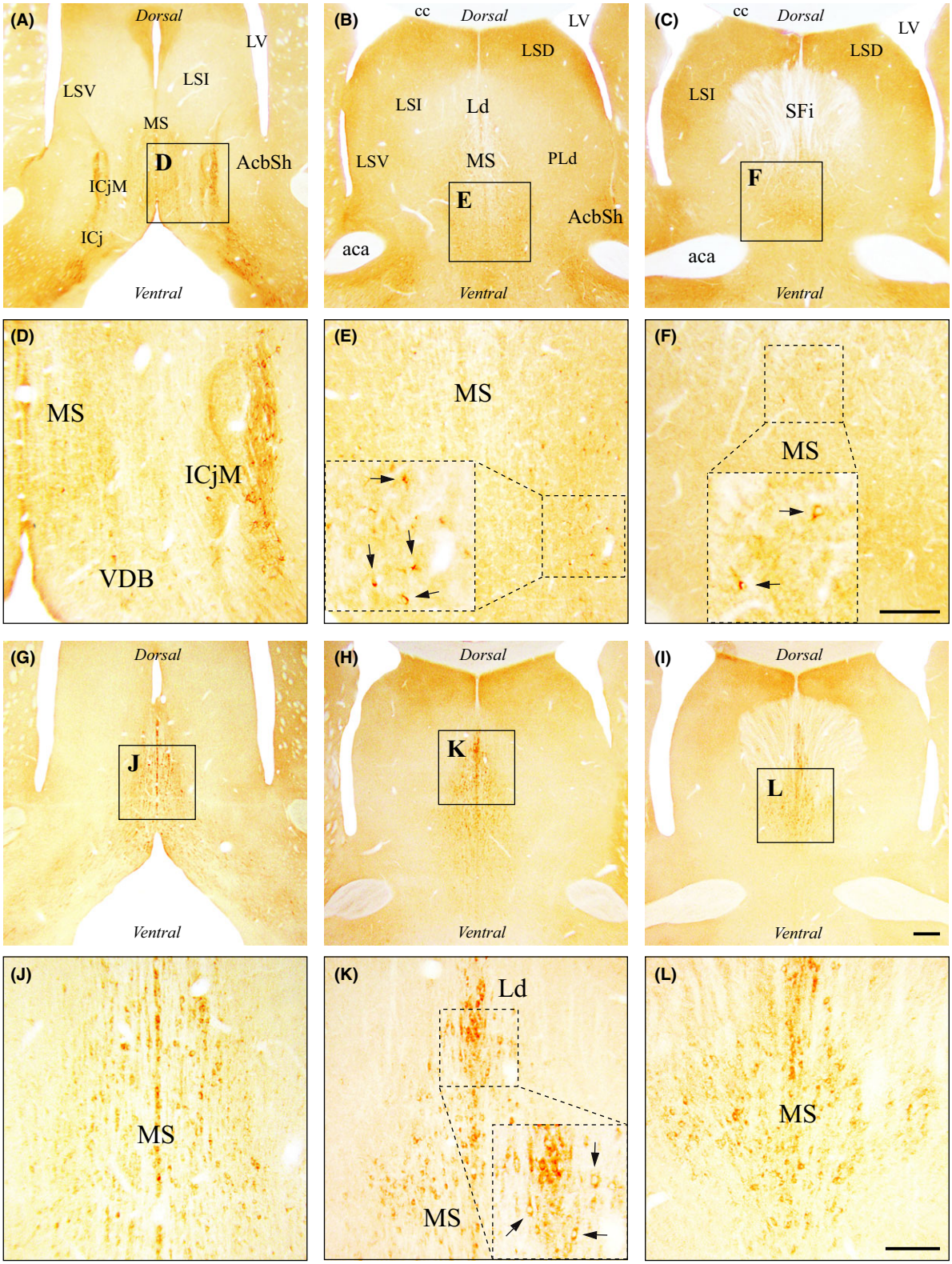

Fig. 5. Immunohistochemical localization of MT_1 and MT_2 receptors in the septal area. (A–F) MT_1 immunoreactivity in the rostral (A, D), middle (B, E), and caudal (C, F) thirds of the septum. As indicated by inserts, high magnifications of A, B, and C are, respectively, shown in D, E, and F. Dashed inserts in E and F illustrate higher magnifications of the medial septum where small MT_1-positive neurons were detected (arrows). (G–L) MT_2 immunoreactivity in the rostral (G, J), middle (H, K), and caudal (I, L) thirds of the septum. High magnifications of G, H, and I are shown, respectively, in J, K, and L. Dashed inserts in K illustrate higher magnifications of the medial septum. Stereotaxic coordinates are bregma 1.44 mm, interaural 10.44 mm (A, D, G, J); bregma 0.48 mm, interaural 9.48 mm (B, E, H, K); bregma 0.00 mm, interaural 9.00 mm (C, F, I, L). See main list for abbreviations. Scale bars: 250 μm in I; 125 μm in F and L.

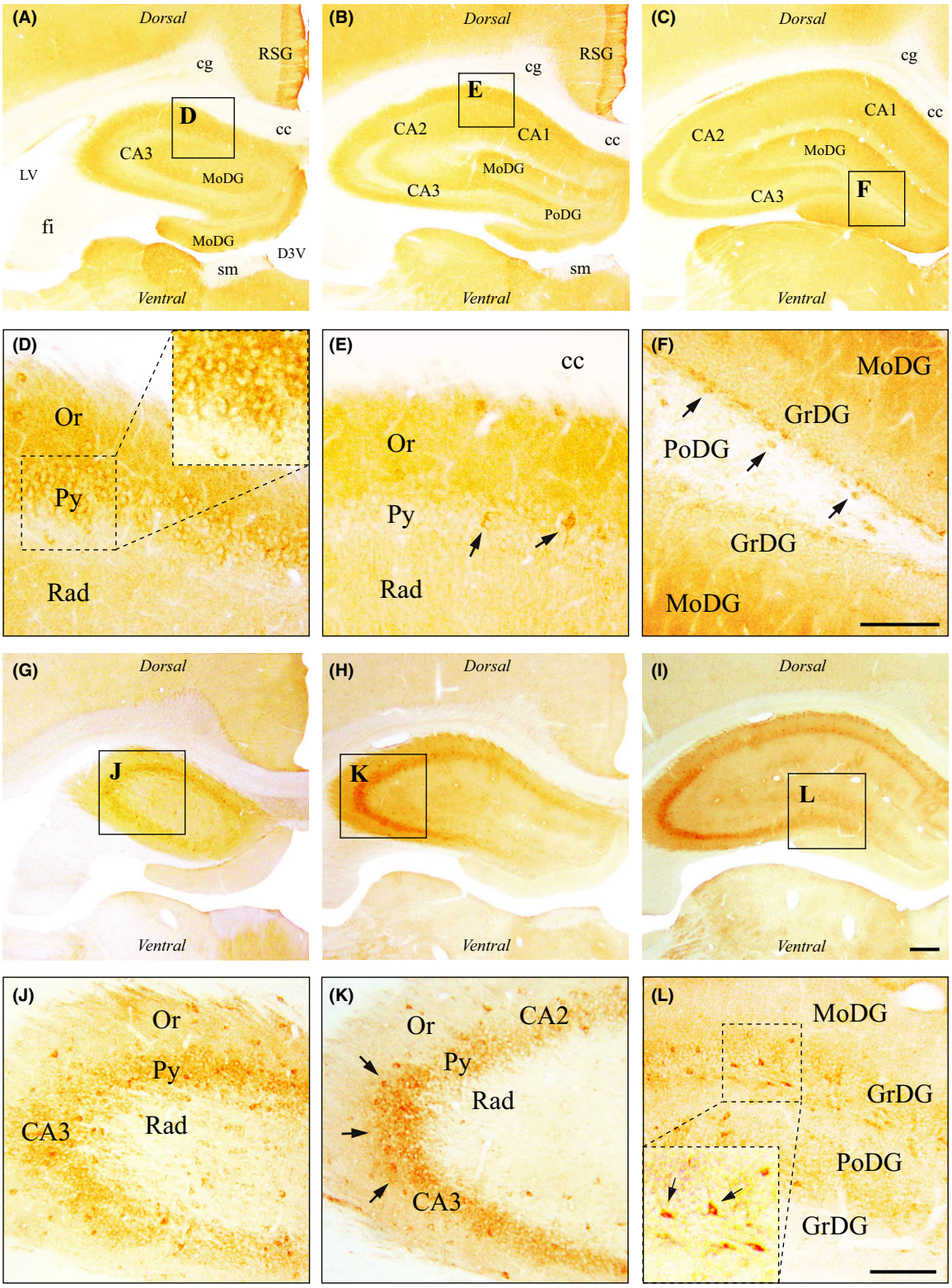

Fig. 6. Immunohistochemical localization of MT_1 and MT_2 receptors in the hippocampal formation. (A–F) MT_1 immunoreactivity in the rostral (A, D), middle (B, E), and caudal (C, F) thirds of the dorsal hippocampus. As indicated by inserts, high magnifications of A, B, and C are shown in D, E, and F, respectively. Few MT_1-positive neurons were found in the CA1 field (dashed inserts in D, arrows in E), as in the hilus of the dentate gyrus (DG) (arrows in F). (G–L) MT_2 immunoreactivity in the rostral (G, J), middle (H, K), and caudal (I, L) thirds of the dorsal hippocampus. High magnifications of G, H, and I are shown, respectively, in J, K, and L. MT_2 labeling reminiscent of interneurons appeared strong in the CA3 field (arrows in K) and generally moderate in the DG (arrows in L). Stereotaxic coordinates are bregma −2.16 mm, interaural 6.84 mm (A, D, G, J); bregma −2.64 mm, interaural 6.36 mm (B, E, H, K); bregma −3.24 mm, interaural 5.76 mm (C, F, I, L). See main list for abbreviations. Scale bars: 250 μm in I; 125 μm in F and L.

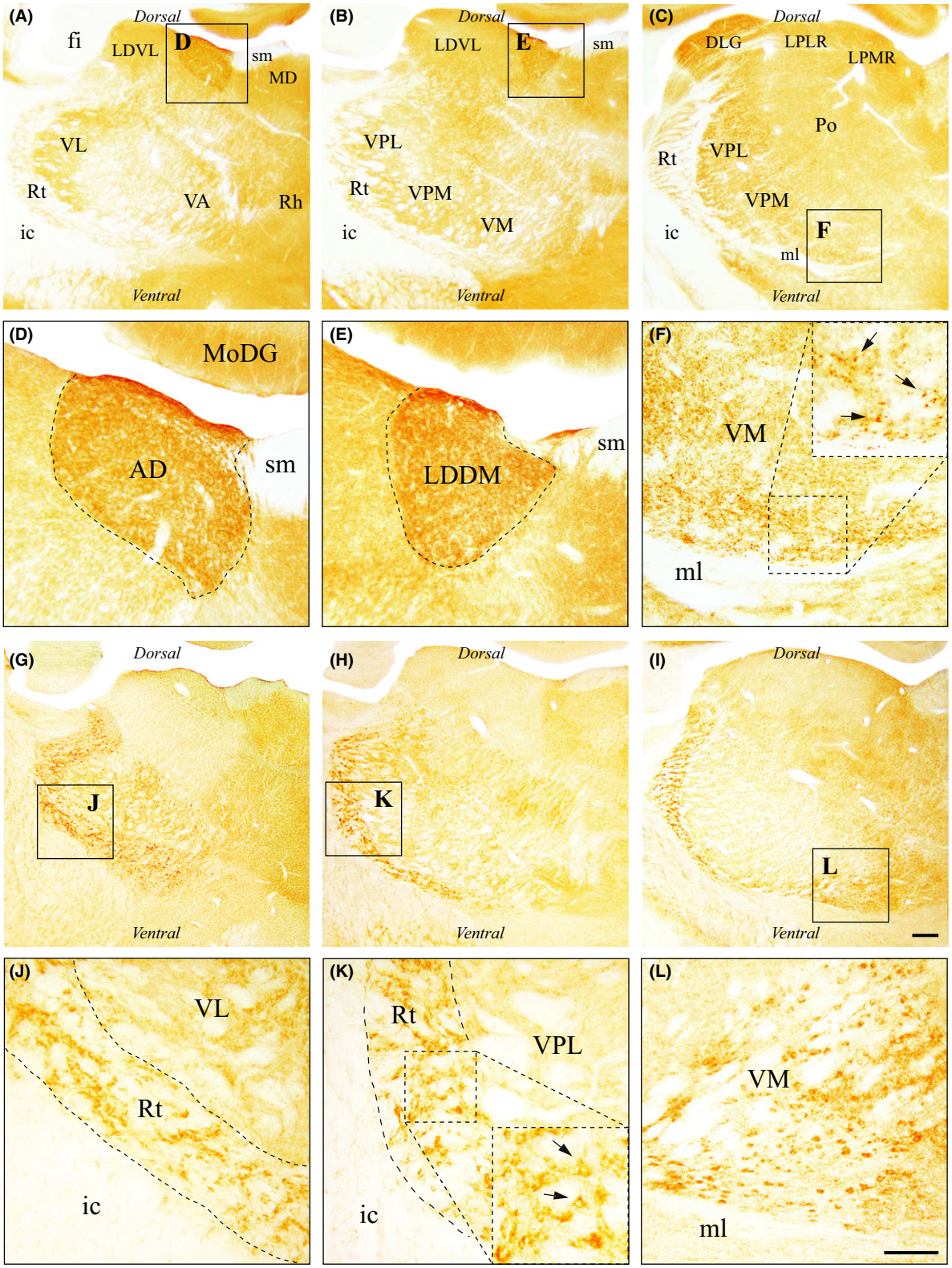

Fig. 7. Immunohistochemical localization of MT_1 and MT_2 receptors in the thalamus. (A–F) MT_1 immunoreactivity in the rostral (A, D), middle (B, E), and caudal (C, F) thirds of the thalamus. As indicated by inserts, high magnifications of A, B and C are shown in D, E, and F, respectively. Dashed inserts in F show cross-sectioned MT_1-positive dendritic profiles (arrows) observed in the ventromedial nucleus. (G–L) MT_2 immunoreactivity in the rostral (G, J), middle (H, K), and caudal (I, L) thirds of the thalamus. High magnifications of G, H, and I are shown, respectively, in J, K, and L. Stereotaxic coordinates are bregma −2.04 mm, interaural 6.96 mm (A, D, G, J); bregma −2.64 mm, interaural 6.36 mm (B, E, H, K); bregma −3.48 mm, interaural 5.52 mm (C, F, I, L). See main list for abbreviations. Scale bars: 250 μm in I; 125 μm in L.

while only MT_1 receptors could be detected in the shell of the nucleus accumbens (AcbSh), particularly in its lateral aspect (LAcbSh). From bregma and caudally, moderate MT_1 and MT_2 immunoreactivity was also found in the VP and in the medial forebrain bundle (mfb; e.g., Fig. 4E,K), while weak to moderate MT_1 immunostaining could be observed in the basal portion of the substantia innominata (SIB; Fig. 4F). Melatonin receptors were absent from several structures of the basal forebrain, like the intermediate endopiriform nucleus (IEn) and both the medial and lateral preoptic areas (respectively, LPO and MPA).

Amygdala

Both melatonin receptors were almost absent from the amygdala complex. Rostrally, where no MT_2 receptor could be detected, MT_1 immunoreactivity was weak in the medial division of the central amygdaloid nucleus (CeM), and moderate in the anteroventral portion of the medial amygdaloid nucleus (MeAV). Caudally, where no MT_1 receptors could be seen, a weak MT_2 labeling density was observed in the amygdalo-piriform transition (APir) and in the posteromedial part of the amygdalo-hippocampal area (AHiPM).

Septal area

Both melatonin receptors were found in distinct structures along the rostrocaudal extent of the septum, but MT_1 immunoreactivity was mainly observed in its rostral aspect, laterally, and MT_2 immunoreactivity along the whole anteroposterior axis, medially (Fig. 5). Rostrally, MT_1 labeling density was strong in the major island of Calleja (ICjM) and only weak in the medial septal nucleus (MS), as in the vertical limb of the diagonal band of Broca (VDB; Fig. 5A,D). In the same areas, moderate MT_2 immunostaining was restricted to the MS and VDB (Fig. 5G,J). Caudally, while MT_2 labeling density stained moderately in the MS and became strong in the lambdoid septal zone (Ld; Fig. 5H,K), MT_1 immunoreactivity decreased to a weak density in the MS (Fig. 5E,F). All other subdivisions of the septum were immunonegative for both melatonin receptors, including the three portions of the lateral septal nucleus (intermediate, LSI; ventral, LSV; and dorsal, LSD).

Hippocampus

As illustrated for the dorsal hippocampus (Fig. 6), a diffuse MT_1 labeling and a more distinct MT_2 labeling were observed in this brain region (Fig. 6 and Table 1). In the CA1 field, few MT_1-positive neurons were found in the pyramidal cell layer (Py), mostly rostrally, while a diffuse MT_1 labeling was observed in the stratum oriens (Or) and radiatum (Rad) (Fig. 6D,E). MT_1 staining density was only weak in the CA2 and weak to moderate in the CA3. MT_2 immunoreactivity suggestive of interneurons, scattered throughout layers [26], appeared of moderate density in the CA1, weak in the CA2, whereas strong labeling density was observed in the CA3 region where MT_2-immunoreactive cell bodies were more concentrated in the Py layer (Fig. 6H,I,K). In the dentate gyrus (DG), only weak and diffuse MT_1 immunoreactivity was observed. MT_1-positive cell bodies were found in the hilus of the DG, scattered in the polymorph layer (PoDG), and precisely aligned along the subgranular zone, while the granular layer (GrDG) remained MT_1-immunonegative (Fig. 6F). As in other parts of the hippocampal formation, MT_2 immunoreactivity was generally moderate in the DG (Fig. 6I,L). Somatodendritic MT_2 labeling could be observed in the hilus, in the inner third of the CA3, as well as in the dorsal portion of the GrDG, while both MoDG and ventral GrDG were MT_2-negative (Fig. 6L). Weak MT_2 immunoreactivity could be found in the PoDG.

Basal ganglia

In telencephalic basal ganglia, namely the striatum (nucleus accumbens, caudate-putamen) and the globus pallidus (GP), low MT_1 and MT_2 receptor immunoreactivity was consistently detected (Table 1). Both receptors were absent from the nucleus accumbens (Acb), except for a weak MT_1 density in the lateral portion of the Acb shell (LAcbSh) where few immunopositive neurons appeared scattered between the anterior commissure and the ICj. In addition, no melatonin receptor whatsoever was found along the whole rostrocaudal extent of the caudate-putamen (striatum). In the GP, however, weak to moderate MT_2 immunostaining was observed. Medial and inferior to the GP, a moderate MT_1 and MT_2 immunoreactivity was detected in the nucleus basalis of Meynert (NBM).

Epithalamus

While MT_2 immunoreactivity was absent from the whole habenular complex, a strong MT_1 labeling density appeared restricted to the medial habenula (MHb; Fig. 3G–L; see also Table 1). In the anterior portion of the habenula, MT_1-positive neurons were found to be numerous in the ventromedial aspect of the MHb (Fig. 3H and insert). In the middle portion of the habenula and caudally, moderate and strong MT_1 labeling density was found in the ventromedial and ventrolateral MHb, respectively (Fig. 3I–L). Only weak MT_1-immunoreactivity could be observed in the lateral habenula (LHb), mainly in its medial half (LHbM).

Thalamus

In general, MT_1 and MT_2 immunostaining appeared complementary in the thalamus (Fig. 7 and Table 1). MT_1 immunoreactivity was almost exclusively associated with dendritic profiles, whereas numerous MT_2 cell bodies could be observed in various areas. In the anterior third of the thalamus, a moderate MT_1 labeling density appeared restricted to the anterodorsal nucleus (AD), immediately lateral to the stria medullaris (sm; Fig. 7A,D). Only weak, diffuse MT_1 immunoreactivity was found in the ventrolateral (VL), ventral anterior (VA), and rhomboid (Rh) nuclei. At the same level, density of MT_2-positive cell bodies and their proximal dendrites was weak in the

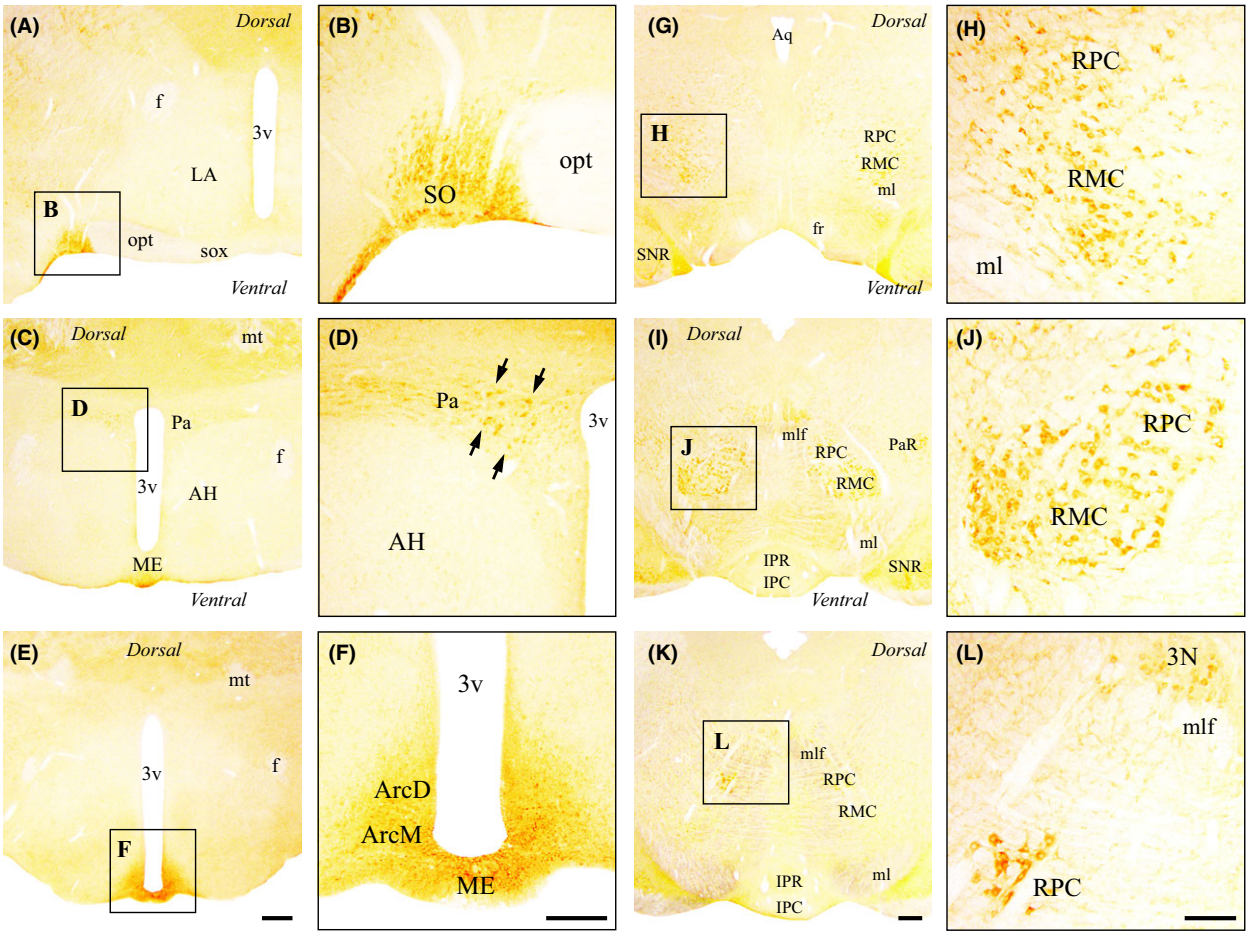

Fig. 8. Anatomical regions mainly or exclusively immunoreactive for the MT_2 receptor. (A–F) rostral (A, B), middle (C, D), and caudal (E, F) thirds of the hypothalamus. As indicated by inserts, high magnifications of A, C, and E are shown in B, D, and F, respectively. MT_2-positive neurons appeared scattered in the paraventricular nucleus (arrows in D). Stereotaxic coordinates are bregma −1.44 mm, interaural 7.56 mm (A, B); bregma −1.80 mm, interaural 7.20 mm (C, D); bregma −3.24 mm, interaural 5.76 mm (E, F). (G–L) rostral (G, H), middle (I, J), and caudal (K, L) thirds of the anterior mesencephalon. High magnifications of G, I, and K are shown, respectively, in H, J, and L. Stereotaxic coordinates are bregma −5.40 mm, interaural 3.60 mm (G, H); bregma −5.88 mm, interaural 3.12 mm (I, J); bregma −6.24 mm, interaural 2.76 mm (K, L). See main list for abbreviations. Scale bars: 250 μm in E, K; 125 μm in F, L.

mediodorsal (MD), central medial (CM), anteromedial (AM), and VL nuclei and moderate in the Rt (Fig. 7G,J). In the middle and posterior thirds of the thalamus, in addition to a moderate MT_1 labeling density in the dorsomedial part of the laterodorsal nucleus (LDDM; Fig. 7B, E), numerous cross-sectioned MT_1-positive dendritic pro-

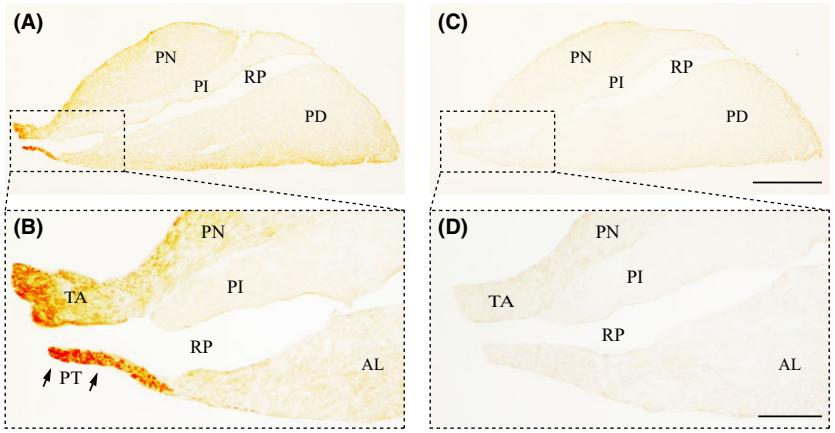

Fig. 9. Immunohistochemical localization of MT_1 and MT_2 receptors in the pituitary gland. (A, B) MT_1 immunoreactivity in the pituitary gland. (C, D) MT_2 immunoreactivity in the pituitary gland. See main list for abbreviations. Scale bars: 500 μm in C; 125 μm in D.

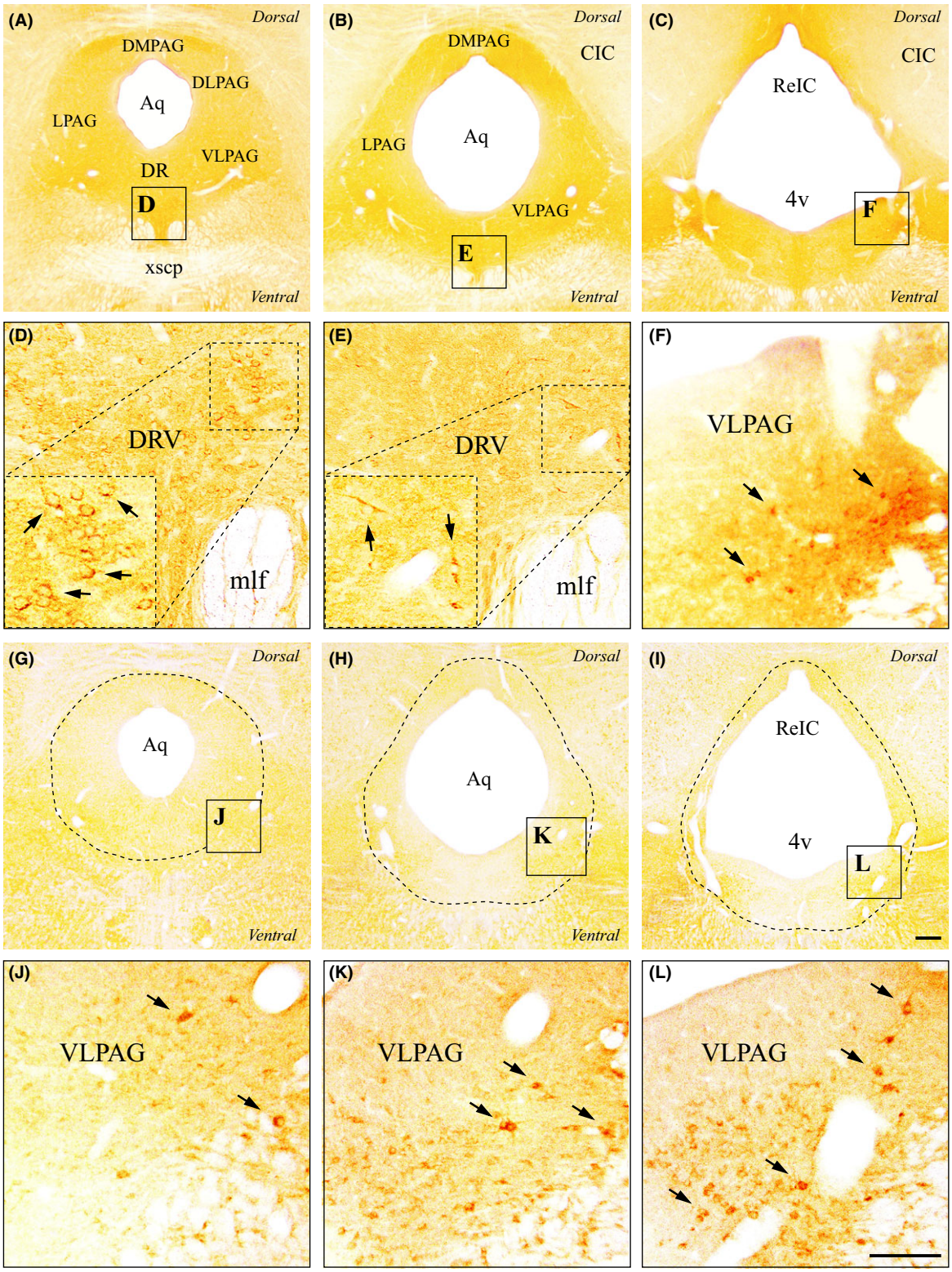

Fig. 10. Immunohistochemical localization of MT_1 and MT_2 receptors in the periaqueductal gray (PAG). (A–F) MT_1 immunoreactivity in the rostral (A, D), middle (B, E), and caudal (C, F) thirds of the PAG matter. As indicated by inserts, high magnifications of A, B, and C are, respectively, shown in D, E, and F. MT_1-positive neurons (arrows in D–F) were observed in the ventromedial aspect of the dorsal raphe nucleus (dashed inserts in D, E) and in the caudal ventrolateral PAG (F). (G–L) MT_2 immunoreactivity in the rostral (G, J), middle (H, K), and caudal (I, L) thirds of the PAG. High magnifications of G, H, and I are shown, respectively, in J, K, and L. MT_2-positive neurons were observed mainly in the ventrolateral PAG (arrows in J–L). Stereotaxic coordinates are bregma −7.80 mm, interaural 1.20 mm (A, D, G, J); bregma −8.40 mm, interaural 0.60 mm (B, E, H, K); bregma −8.64 mm, interaural 0.36 mm (C, F, I, L). See main list for abbreviations. Scale bars: 250 μm in I; 125 μm in L.

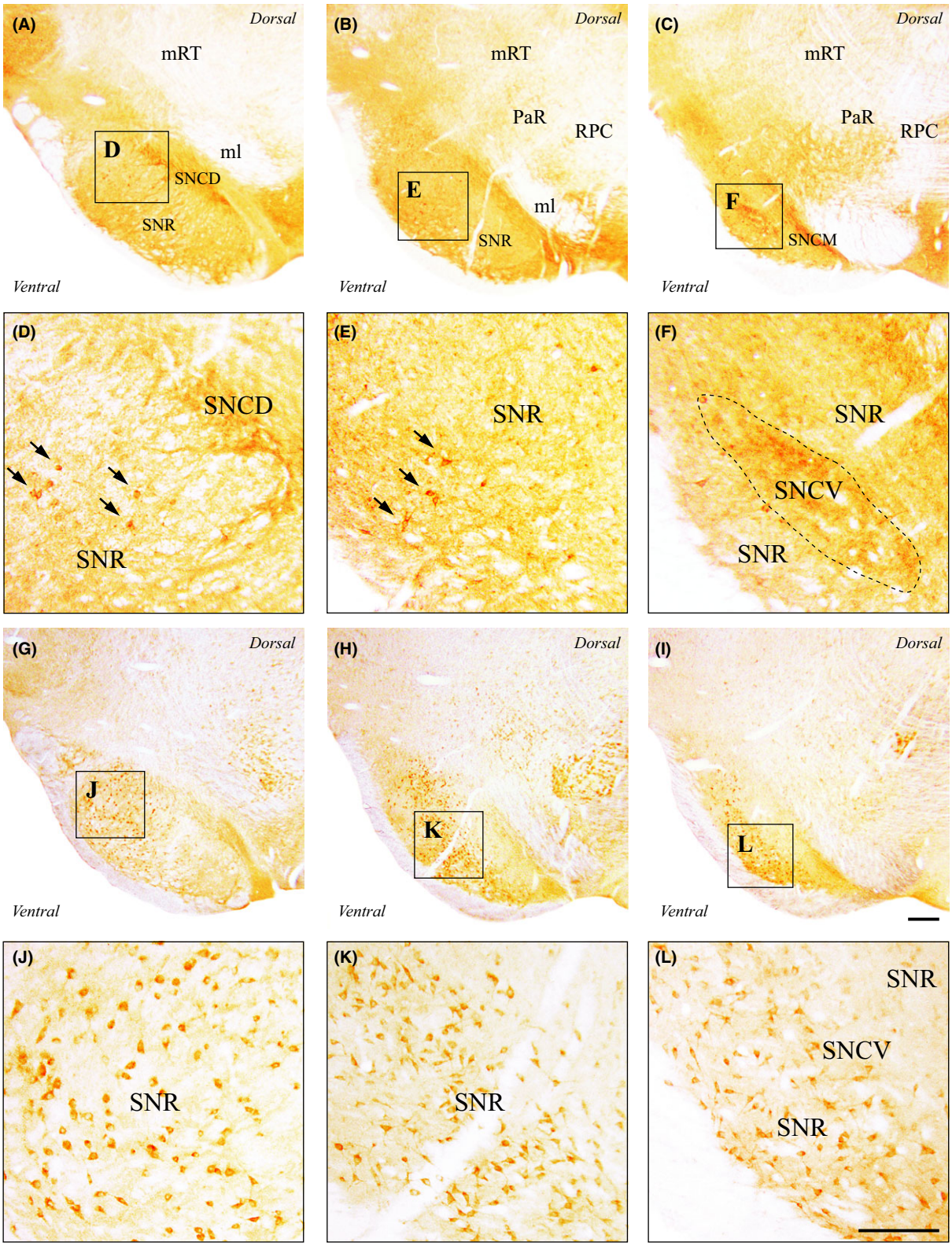

Fig. 11. Immunohistochemical localization of MT_1 and MT_2 receptors in the substantia nigra. (A–F) MT_1 immunoreactivity in the rostral (A, D), middle (B, E), and caudal (C, F) thirds of the substantia nigra (SN). As indicated by inserts, high magnifications of A, B, and C are, respectively, shown in D, E, and F. MT_1-positive somas were mostly observed in the SN *pars reticulata* (arrows in D, E) but also in the SN *pars compacta* whose ventral part is outlined in F. (G–L) MT_2 immunoreactivity in the rostral (G, J), middle (H, K), and caudal (I, L) thirds of the SN. High magnifications of G, H, and I are shown, respectively, in J, K, and L. Stereotaxic coordinates are bregma −5.40 mm, interaural 3.60 mm (A, D, G, J); bregma −5.88 mm, interaural 3.12 mm (B, E, H, K); bregma −6.24 mm; interaural 2.76 mm (C, F, I, L). See main list for abbreviations. Scale bars: 250 μm in I; 125 μm in L.

Table 1. Distribution of MLT receptors immunoreactivity in the adult rat brain

Selected brain regions	MT_1 density	MT_2 density
Telencephalon		
Cerebral cortex		
Prefrontal	+	– (+)
Retrosplenial	+++	+
Occipital	+	–
Basal forebrain		
Islands of Calleja	+++	+
Medial forebrain bundle	++	++
Ventral pallidum	++	++
Hippocampus		
CA1	+	+
CA2	+	+ (+)
CA3	+ (+)	+++
Dentate gyrus	+	++
Basal ganglia		
Nucleus accumbens	– (+)	–
Caudate-putamen	–	–
Globus pallidus	+	+ (+)
Diencephalon		
Epithalamus		
Lateral habenula	+	–
Medial habenula	+++	–
Thalamus		
Anterodorsal nucleus	++	–
Reticular nucleus	–	+++
Ventromedial nucleus	+	++
Hypothalamus		
Paraventricular nucleus	–	+
Supraoptic nucleus	–	+++
Medial eminence	+	++
Suprachiasmatic nucleus	++ (+)	–
Mesencephalon		
Dorsal mesencephalon		
Superior colliculi	+++	+
Inferior colliculi	++ (+)	++ (+)
PAG		
Ventrolateral PAG	+	++
Dorsal raphe nucleus	++	+
Ventral mesencephalon		
Substantia Nigra *pars compacta*	++ (+)	+
Substantia Nigra *pars reticulata*	+	++ (+)
Pituitary gland		
Pars tuberalis	+++	–

PAG, periaqueductal gray. Semiquantitative estimates of immunocytochemical density are denoted as: –, no immunostaining; +, weak; ++, moderate; +++, strong; intermediate levels are indicated in brackets.

files could be observed in the dorsal lateral geniculate, ventral posterolateral (VPL), ventral posteromedial (VPM), and ventromedial (VM) nuclei (Fig. 7F). Few MT_1-positive cell bodies were found in the CM and Rh nuclei, and more abundantly in the caudal half of the submedius nucleus. In the same area, MT_2 labeling density was weak in the centrolateral (CL), MD, VPM, and posterior thalamic (Po) nuclei, moderate in the caudal part of the VL nucleus, but strong in the Rt and VM nuclei (Fig. 7K,L). Both melatonin receptors were absent from various dorsal thalamic nuclei, like the paraventricular (PV), ventrolateral laterodorsal (LDVL), and lateroposterior (LPLR and LPMR) nuclei.

Hypothalamus

Rostrally, few MT_1-positive somadendrites were observed in the peduncular part of the lateral hypothalamus (PLH). While the suprachiasmatic nucleus (SCh) displayed a moderate to strong MT_1 density (Fig. 1D), only few MT_1-positive neurons were detected caudally in its ventromedial division (SChVM). In the same anterior hypothalamic segment, MT_2 labeling density was weak in the ventral PLH, moderate in the magnocellular preoptic (MCPO), and strong in the supraoptic (SO) nuclei (Fig. 8A,B). Caudally, MT_1 labeling density was very weak in the dorsal dorsomedial (DMD), perifornical (Pe), and submammillothalamic (SMT) nuclei. MT_2 labeling was weak in the perifornical area and moderate in the paraventricular nucleus (PaV) and medial eminence (ME) (Fig. 8C–F). Melatonin receptor immunoreactivity was absent from other hypothalamic areas.

Pituitary

The pituitary gland, lodged in the hypophyseal fossa and connected to the base of the hypothalamus by the infundibulum (Inf), displayed a very specific pattern of melatonin receptor staining (Fig. 9). While the pars nervosa (PN), pars intermedia (PI), and pars distalis (PD) were MT_1- and MT_2-immunonegative (Fig. 9A–D), both the pars tuberalis (PT) and the transitional area (TA) between the PN and the Inf displayed a moderate to strong MT_1 labeling density (Fig. 9A,B).

Dorsal mesencephalon

MT_1- and MT_2-positive cellular elements were detected in both the superior (SC) and inferior (IC) colliculi (Table 1). Rostrally, in the dorsal aspect of the SC, a region deprived of MT_2 immunoreactivity, a dense network of MT_1-positive dendrites was observed in the zonal (Zo) and superior gray (SuG) layers, even denser along the medial line. MT_1 labeling density appeared moderate in the optic nerve layer (Op) and almost absent from the ventral SC layers (InG, intermediate gray; InWh, intermediate white; DpG, deep gray; DpWh, deep white). MT_2 labeling density of cellular bodies and their proximal dendrites was weak in the Op and moderate in the InG. Caudally, MT_1- and MT_2-immunoreactive somadendrites were detected in various subdivisions of the IC. While only a weak MT_2 labeling density could be observed in superficial (cortical) layer 1 of the IC, melatonin receptor density appeared weak to moderate in cortical layers 2 and 3, as in the external and dorsal IC cortices (respectively, ECIC and DCIC).

Periaqueductal gray

In the rostral third of the periaqueductal gray (PAG), MT_1 labeling density was weak in the dorsomedial (DMPAG), dorsolateral (DLPAG), lateral (LPAG), and ventrolateral (VLPAG) subdivisions, but moderate in the dorsal raphe nucleus (DR) where MT_1-positive neurons were densely packed in the ventral aspect of the nucleus

(DRV) and in between the medial longitudinal fasciculi (mlf; Fig. 10A,D; see also Table 1). In the same region, MT_2 immunoreactivity was absent from the DMPAG, DLPAG, and LPAG, but a weak MT_2 labeling density was could be observed in the VLPAG (Fig. 10J), as in the DR, where only few cell bodies appeared scattered across the nucleus. The overall distribution of melatonin receptor immunoreactivity in the middle third of the PAG was similar, except that MT_1 labeling density was weaker in the DRV (Fig. 10E) and MT_2 immunostaining slightly denser in the VLPAG (Fig. 10K,L). In the caudal third, where the dorsal and lateral PAG subdivisions consist of a thin layer, MT_1 immunoreactivity became moderate in the VLPAG (Fig. 10F) and almost absent from the DR, while MT_2 labeling density was moderate to strong in the VLPAG (Fig. 10L).

Ventral mesencephalon

In the rostral half of the mesencephalon, posterior to the subthalamic area and ventral to the mesencephalic reticular formation (mRT), melatonin receptor immunoreactivity was particularly obvious in the substantia nigra (SN; Fig. 11 and Table 1). A dense MT_1 immunostaining was observed in the dorsal, medial, and ventral tiers of the SN *pars compacta* (respectively, SNCD, SNCM, and SNCV; Fig. 11A–F). In SNC, MT_1 immunoreactivity was almost exclusively dendritic, with few MT_1-positive cell bodies detected. In the SN *pars reticulata* (SNR), several MT_1-positive neurons were seen, particularly in the lateral and ventral SNR (Fig. 11D,E). MT_2 labeling density was almost null in the SNC and appeared moderate to strong in the SNR, with clearly distinguishable immunopositive somadendrites (Fig. 11G–L). Despite being present along the whole rostro-caudal extent of the SNR, MT_2-positive neurons were more frequently observed in the lateral SNR, rostrally (Fig. 11G,J), and in the ventral SNR, caudally (Fig. 11I,L). Dorsomedial to the SN, MT_2 immunostaining was particularly dense in the oculomotor (3N) and pararubral (PaR) nuclei, as well as in the magnocellular (RMC) and parvocellular (RPC) parts of the red nucleus (Fig. 8G–L). Medially, a weak MT_1 immunoreactivity could be observed in the rostral and lateral interpeduncular subnuclei (IPR and IPC), two regions that appeared MT_2-negative (Fig. 8I,K). In the ventral tegmental area (VTA), both melatonin receptors were found at a very low staining density. Finally, in the caudal half of the mesencephalon, posterior to the SC and ventral to the mlf, several structures were MT_1- and/or MT_2-immunopositive. Principally, from rostral to caudal, MT_1 labeling density appeared weak in the oral part of the pontine reticular nucleus (PnO) and moderate in the median raphe (MnR), medial paralemniscal (MPL), and ventral tegmental (VTg) nuclei. MT_2 labeling density appeared weak in the subpeduncular tegmental (SPTg), reticulotegmental (RtTg), and MnR nuclei, moderate in the PnO, and strong in the VTg.

Cellular localization of melatonin receptors

Immunogold labeling examined by electron microscopy confirmed the exclusive somatodendritic localization of melatonin receptors, with the detection of immunoreactive cell bodies and dendrites only (Fig. 12). Ultrastructurally, as expected for G-protein-coupled receptors, both MT_1 (Fig. 12A–F) and MT_2 (Fig. 12G–L) appeared mainly localized at the plasma membrane, with only a small proportion of cytoplasmic localization that increased toward the cell body. In all regions examined, the cytoplasmic proportion of immunogold particles was generally low, but slightly higher for the MT_2 receptor.

Discussion

This study is the first attempt to describe, using immunohistochemistry, the neuroanatomical and subcellular localization of both melatonin MT_1 and MT_2 receptor proteins across the rat brain. Previous studies have reported the existence of high-affinity binding sites for melatonin or localized mRNA expression of melatonin receptors [27]. But until now, the lack of selective antibodies for the detection of MT_1 and MT_2 proteins has restricted the knowledge about the sites of action of melatonin in the CNS. Here, we detected the presence of each receptor in numerous brain regions, and we found that both MT_1 and MT_2 receptors are expressed by neurons, but not by glial cells. We confirmed the presence of MT_1 and/or MT_2 receptors in areas previously known for their high concentration in melatonin binding sites, such as the SCh [28–31] and the *pars tuberalis* of the pituitary gland [32–36], and we found a distinct presence of MT_1 and MT_2 receptor proteins in different brain areas suggesting a distinctive localization and thus function of each receptor in neurophysiological and neuropathological contexts [2].

With immunohistochemistry, melatonin receptor immunolabeling was found in numerous brain regions. Originally, melatonin binding sites in the rat pituitary gland and brain were described predominantly in the median eminence, the SCh, the area postrema, the paraventricular thalamic nucleus, as well as the hypothalamus, the hippocampus, the parietal cortex, and the striatum [37–39]. More binding sites were later added to the list, including the *pars tuberalis* of the pituitary gland, the medial region of the lateral habenula, the arcuate nucleus, and the amygdala [40]. MT_1 receptor mRNA has been detected in the rodent dorsal striatum, nucleus accumbens, olfactory tubercle, substantia nigra, and ventral tegmental area (VTA) [41]. MT_1 and MT_2 receptor mRNA expressions have been reported in the SCN and vestibular nuclei [42, 43]. In humans, MT_1 mRNA and protein have been detected in areas including the hypothalamus, the cerebellum, the frontal cortex, the nucleus accumbens, the amygdala, and hippocampus [13, 34, 41, 44], and MT_2 receptor transcripts were described in the hippocampus [45]. Noteworthy, certain variability across species has been noticed for melatonin receptors localization [46].

Melatonin has been implicated in the control of several physiological processes by direct action on its G-protein couple receptors [47]. One of the most studied functions of melatonin is the regulation of sleep. Here, we confirmed the presence of MT_2 receptors in the reticular thalamic nucleus, where they mediate neuronal firing and burst activity related to the NREM sleep [10]. Moreover, we

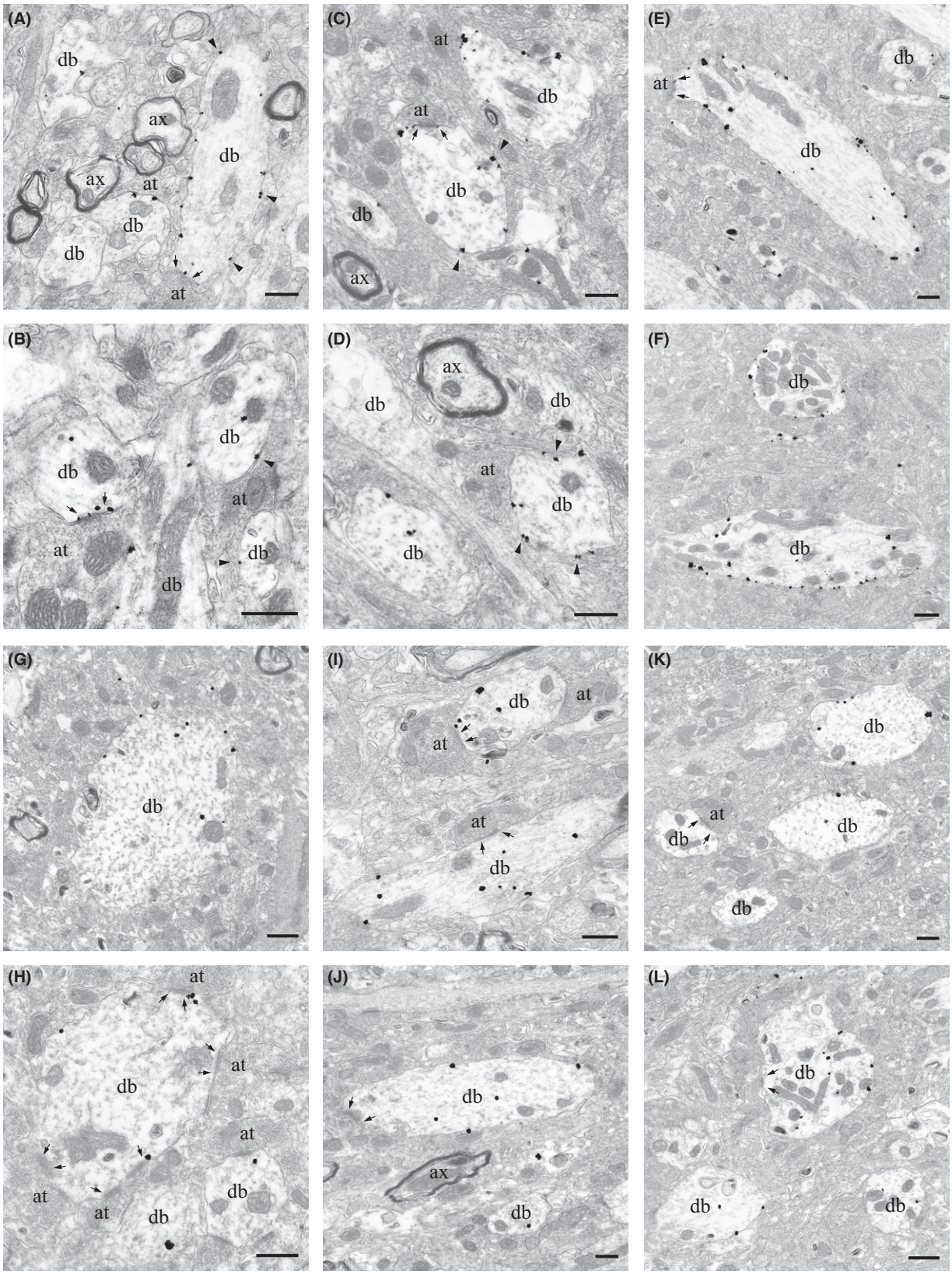

Fig. 12. Ultrastructural features of MT_1 and MT_2 receptors in selected brain areas. (A–F) MT_1 immunogold labeling in the retrosplenial cortex (A, B), dorsal raphe nucleus (C, D), and substantia nigra *pars compacta* (E, F). Generally, the membrane density of MT_1 receptors appeared higher in the SN. (G–L) MT_2 immunogold labeling in the hippocampus (G, H), ventrolateral PAG (I, J), and substantia nigra *pars reticulata* (K, L). Both melatonin receptors are exclusively somatodendritic and mainly membrane-bound (gold particles, arrowhead as examples). Synaptic contacts are enclosed between small arrows, at: axon terminal; ax: axon; db: dendritic body. Scale bars: 500 nm.

report the lack of MT_1 receptors in this area, confirming the high specificity of melatonin receptor function in sleep neurophysiology. Polysomnographic studies in MT_1, MT_2, and double MT_1-MT_2 knockout mice have indeed shown that both receptors have complementary or opposite effects [48], MT_2 receptors being involved in NREM sleep, whereas MT_1 receptors in rapid eye movement (REM) sleep [10, 48]. The presence of MT_1 in the lateral hypothalamus [49] as well as in the superior colliculi, that sends projections to the paramedian pontine reticular formation (PPRF), which in turn coordinates the duration and direction of REM eye movements [50], strongly reinforces the hypothesis of the involvement of this receptor in REM. Previous binding studies also indicated the presence of melatonin binding sites in the thalamus, in particular the rat anteroventral and anterodorsal thalamic nuclei [51], with similar expression patterns of MT_1 and MT_2 as observed in our experiments.

For the first time, we detected an abundant presence of MT_1, but not MT_2, receptors in the dorsal raphe (DR), the major source of 5-HT neurons that are involved in the pathophysiology of depression and mood disorders [52]. In agreement with these findings, MT_1 receptors knockout (but not MT_2 knockout) mice show a depressive-melancholic phenotype with circadian impairment of high firing 5-HT neurons of the DR [53]. Furthermore, an inhibitory modulation of the 5-HT firing activity in the DR, mediated by MT_1 receptors, was also reported by our group [54].

Melatonin binding sites in the mammalian hypothalamus have been previously described and, predominantly, melatonin actions on the premammilar area have been linked to the control of the reproductive axis through modulation of luteinizing hormone secretion [55]. We found that both MT_1 and MT_2 receptors have a specific distribution across the hypothalamus. MT_1 receptors were observed in the lateral hypothalamus and the medial eminence, which may indicate a direct role of MT_1 receptors in the GnRH pulse generator [56]. The presence of MT_1 receptors in the SCh has previously been observed in the rat brain following in situ hybridization [43], and in the human brain using immunohistochemistry [34], supporting the role of melatonin on regulating biological circadian rhythms. In our experiments, while confirming the presence of MT_1 receptors in the SCh, we could not detect a significant amounts of the MT_2 protein in this region, which is consistent with the absence of in situ hybridization signal in this nucleus [43]. MT_2 labeling was observed in the paraventricular nucleus, magnocellular preoptic, and supraoptic nuclei, areas involved directly and indirectly in the secretion of oxytocin and vasopressin, supporting a role of melatonin in the control of uterine contractions and parturition [57].

We observed lower levels of MT_1 immunoreactivity across the different subdivisions of the hippocampal formation. In line with this, previous studies reported low MT_1 protein and mRNA expression in pyramidal cell of hippocampal human tissue [44, 58]. In contrast, MT_2 receptors seem to have a denser representation in the hippocampus, as previously reported in humans [19]. Other studies have reported that MT_1 and MT_2 receptor transcripts are predominately expressed in hippocampal layers CA1 and CA3 as well as in the DG [45], which is consistent with our observations. In addition, similar to what we found in the cerebral cortex at the protein level, lower MT_1 mRNA levels have been reported in the prefrontal and temporal cortices and higher levels in the parietal and occipital cortices [44]. Melatonin receptor labeling is also known to be restricted to human cortical layers II–IV and absent from layer I [59]. However, we observed a preferential MT_1 labeling in the layers II/III and V, and MT_2 labeling in layers V and VI. Noteworthy, abnormal expression of melatonin receptors, especially MT_2, in the hippocampus and cortex has been related to neurodegenerative processes that affect cognition such as Alzheimer disease [19, 58, 59].

Several studies have suggested that melatonin modulates dopaminergic system, decreasing firing of VTA dopamine neurons in both light and dark phases [60], and influencing the response to psychostimulants such as amphetamine and cocaine [61, 62]. We were able to detect MT_1 immunoreactive cells in the lateral portion of the nucleus accumbens shell (LAcbSh), and both receptors were detected in the VTA. Accordingly in mice, neurons located in the nucleus accumbens expressing D_2 dopamine receptors and neurons located in the VTA expressing TH are also positive for MT_1 mRNA [41].

Recently, a *postmortem* study reported a decrease in the expression (mRNA level) of both MT_1 and MT_2 receptors in the substantia nigra (SN) of Parkinson's disease patients [63]. Interestingly, this finding is in accordance with our observation of high MT_1 receptor labeling densities in the two subdivisions (*pars compacta* and *pars reticulata*) of the SN. Furthermore, the expression of MT_2 receptors in the SN *pars reticulata*, the red nucleus, the oculomotor, pararubral nuclei, the GP, and the colliculi suggests that this receptor might be involved in the motor effects of systemic administration of melatonin in these areas [64]. Yet, more studies are needed to dissect the involvement of melatonin in movement disorders.

Our findings demonstrate the presence of the MT_1 protein in the AcbSh, CeM, MeAV, and SChVM, and of the MT_2 protein in the APir and AHiPM. In keeping with these results, a constant inhibitory effect of exogenous melatonin administration has been observed in other neuronal areas including the mesencephalic reticular formation, the striatum, the amygdala, and SCh [65–68].

Recent studies have affirmed the role of MT_2 receptor in the control of inflammatory [69] and neuropathic pain [70]. These pharmacological and physiological properties of melatonin are supported by the presence of MT_2 receptors in brain areas involved in pain processing (PAG) [71], specifically they are localized in the glutamatergic neurons of PAG, controlling the activity of ON and OFF cells of the descending nociceptive pathways [70].

MT_1 and MT_2 receptors were localized in areas known to be implicated in anxiety and stress such as the septal area, habenula, hippocampus, and DG [72, 73]. High doses of melatonin and low doses of the selective MT_2 agonist UCM765 showed anxiolytic-like effects in animal models of anxiety, similar to the benzodiazepine diazepam, but without its locomotor side effects [74].

One limitation of the study is not having used the MT_1 and MT_2 knockout as a control for these polyclonal anti-

bodies. Unfortunately, knockout mice available are functional knockout; the MT_1 knockout have a deletion of the exon 1 from the MT_1 gene, whereas exon 2 is still present [11], which may well produce nonfunctional truncated proteins likely stained by our antibodies [34]. Similarly, in the MT_2 knockout mice, the first exon of the MT_2 receptor gene was disrupted resulting in inactivation of the gene, but some of the receptorial protein can be still expressed [75].

In conclusion, this study is the first to describe the regional and cellular localization of melatonin somatodendritic receptors MT_1 and MT_2 in the rat brain. The different localization of MT_1 and MT_2 receptors in various brain regions is suggestive of their functional specialization in the control of several physiological functions. The elucidation of the role of each of these receptors in brain physiology and pathophysiology will open novel opportunities for the development of selective MT_1 and MT_2 receptor ligands.

Acknowledgements

The authors also thank Ginette Gay for technical assistance (ultrathin sectioning) and Pr. Maria L. Vitale for her precious advises on pituitary extraction. This work was supported by grants from the Fonds de la Recherche en Santé du Quebec (FRSQ, to G.G., L.D.), the Canadian Institutes of Health Research (CIHR) to G.G. (PPP-81421; PP2-90159) and L.D., the McGill University Health Center (MUHC, to G.G.,), the Ministère du Développement Économique, Innovation et Exportation (MDEIE, to G.G.).

Authors contribution

BL, LD, and GG contribute to study concept and design. BL, DA, and SC contribute to acquisition of data. BL, DA, SD-L, and GG contribute to analysis and interpretation of data. BL, SD-L, DA, SC and GG involved in drafting of the manuscript. LD, GG, and FF involved in critical revision of the manuscript for important intellectual content. LD and GG obtained funding. FF, LD, and AM involved in technical, and material support. LD and GG involved in study supervision.

Abbreviations

(Index of anatomical structures in alphabetic order, from the stereotaxic atlas of Paxinos and Watson, [76])

3N	oculomotor nucleus
3v	3rd ventricle
4v	4th ventricle
I, II, III	cortical layers
AA	anterior amygdaloid area
aca	anterior commissure, anterior
AcbC	accumbens nucleus, core
AcbSh	accumbens nucleus, shell
acp	anterior commissure, posterior
AD	anterodorsal thalamic nucleus
AH	anterior hypothalamic area
AL	pituitary, anterior lobe
APir	amygdalo-piriform transition
AHiPM	amygdalo-hippocampal area, posteromedial part
Aq	aqueduct
ArcD	arcuate hypothalamic nucleus, dorsal part
ArcM	arcuate hypothalamic nucleus, medial part
CA1, CA2, CA3	fields CA1,2,3 of the hippocampus
cc	corpus callosum
CeM	central amygdaloid nucleus, medial part
CIC	central nucleus of the inferior colliculus
cg	cingulum
CPu	caudate-putamen (dorsal striatum)
D3V	dorsal 3rd ventricle
DLPAG	dorsolateral periaqueductal gray
DLG	dorsal lateral geniculate nucleus
DMPAG	dorsomedial periaqueductal gray
DR	dorsal raphe nucleus
DRV	dorsal raphe nucleus, ventral part
f	fornix
fi	fimbria of the hippocampus
fr	fasciculus retroflexus
GP	globus pallidus
GrDG	granular layer of the dentate gyrus
ic	internal capsule
ICj	islands of Calleja
ICjM	islands of Calleja, major island
IEn	intermediate endopiriform nucleus
Inf	infundibulum
IPC	interpeduncular nucleus, caudal subnucleus
IPR	interpeduncular nucleus, rostral subnucleus
LA	lateroanterior hypothalamic nucleus
LAcbSh	lateral accumbens shell
Ld	lambdoid septal zone
LDDM	laterodorsal thalamic nucleus, dorsomedial part
LDVL	laterodorsal thalamic nucleus, ventrolateral part
LHbL	lateral habenular nucleus, lateral
LHbM	lateral habenular nucleus, medial
LPAG	lateral periaqueductal gray
LPLR	lateral posterior thalamic nucleus, laterorostral part
LPMR	lateral posterior thalamic nucleus, mediorostral part
LPO	lateral preoptic area
LSD	lateral septal nucleus, dorsal part
LSI	lateral septal nucleus, intermediate part
LSV	lateral septal nucleus, ventral part
LV	lateral ventricle
M2	secondary motor cortex
MD	mediodorsal thalamic nucleus
ME	median eminence
MeAV	medial amygdaloid nucleus, anteroventral part
mfb	medial forebrain bundle
MHb	medial habenular nucleus
ml	medial lemniscus
mlf	medial longitudinal fasciculus
MoDG	molecular layer of the dentate gyrus
MPA	medial preoptic area
mRT	mesencephalic reticular formation
MS	medial septal nucleus
mt	mammillothalamic tract

opt	optic tract
Or	Stratum oriens of the hippocampus
Pa	paraventricular hypothalamic nucleus
PaR	pararubral nucleus
PD	pituitary, pars distalis
PI	pituitary, pars intermedia
PLd	paralambdoid septal nucleus
PN	pituitary, pars nervosa
Po	posterior thalamic nuclear group
PoDG	polymorph layer of the dentate gyrus
PT	pituitary, pars tuberalis
PVP	paraventricular thalamic nucleus, posterior
Py	pyramidal cell layer of the hippocampus
Rad	Stratum radiatum of the hippocampus
Rh	rhomboid nucleus
RMC	red nucleus, magnocellular part
RP	pituitary, Rathke's pouch
RPC	red nucleus, parvicellular part
Rt	reticular thalamic nucleus
RSD	retrosplenial dysgranular cortex
RSG	retrosplenial granular cortex
SCh	suprachiasmatic nucleus
SChVM	suprachiasmatic nucleus, ventromedial part
SFi	septofimbrial nucleus
SIB	substantia innominata, basal
sm	stria medullaris
SNR	substantia nigra, reticular part
SNC	substantia nigra, compacta part
SNCD	substantia nigra, compact part, dorsal tier
SNCM	substantia nigra, compact part, medial tier
SNCV	substantia nigra, compacta part, ventral tier
SO	supraoptic nucleus
sox	supraoptic decussation
Tu 1,2,3	olfactory tubercle cortical layers 1,2,3
VA	ventral anterior thalamic nucleus
VDB	nucleus of the vertical limb of the diagonal band
VL	ventrolateral thalamic nucleus
VLPAG	ventrolateral periaqueductal gray
VM	ventromedial thalamic nucleus
VP	ventral pallidum
VPL	ventral posterolateral thalamic nucleus
VPM	ventral posteromedial thalamic nucleus

References

1. Reiter RJ, Tan DX, Kim SJ et al. Delivery of pineal melatonin to the brain and SCN: role of canaliculi, cerebrospinal fluid, tanycytes and Virchow-Robin perivascular spaces. Brain Struct Funct 2014; **219**:1873–1887.
2. Comai S, Gobbi G. Unveiling the role of melatonin MT2 receptors in sleep, anxiety and other neuropsychiatric diseases: a novel target in psychopharmacology. J Psychiatry Neurosci 2014; **39**:6–21.
3. Galano A, Tan DX, Reiter RJ. On the free radical scavenging activities of melatonin's metabolites, AFMK and AMK. J Pineal Res 2013; **54**:245–257.
4. Zhang HM, Zhang Y. Melatonin: a well-documented antioxidant with conditional pro-oxidant actions. J Pineal Res 2014; **57**:131–146.
5. Mauriz JL, Collado PS, Veneroso C et al. A review of the molecular aspects of melatonin's anti-inflammatory actions: recent insights and new perspectives. J Pineal Res 2013; **54**:1–14.
6. Dubocovich ML, Markowska M. Functional MT1 and MT2 melatonin receptors in mammals. Endocrine 2005; **27**:101–110.
7. Morgan PJ, Williams LM. Central melatonin receptors: implications for a mode of action. Experientia 1989; **45**:955–965.
8. Rosales-Corral SA, Acuna-Castroviejo D, Coto-Montes A et al. Alzheimer's disease: pathological mechanisms and the beneficial role of melatonin. J Pineal Res 2012; **52**:167–202.
9. Patki G, Lau YS. Melatonin protects against neurobehavioral and mitochondrial deficits in a chronic mouse model of Parkinson's disease. Pharmacol Biochem Behav 2011; **99**:704–711.
10. Ochoa-Sanchez R, Comai S, Lacoste B et al. Promotion of non-rapid eye movement sleep and activation of reticular thalamic neurons by a novel MT2 melatonin receptor ligand. J Neurosci 2011; **31**:18439–18452.
11. Liu C, Weaver DR, Jin X et al. Molecular dissection of two distinct actions of melatonin on the suprachiasmatic circadian clock. Neuron 1997; **19**:91–102.
12. Reppert SM, Weaver DR, Rivkees SA et al. Putative melatonin receptors in a human biological clock. Science 1988; **242**:78–81.
13. Weaver DR, Stehle JH, Stopa EG et al. Melatonin receptors in human hypothalamus and pituitary: implications for circadian and reproductive responses to melatonin. J Clin Endocrinol Metab 1993; **76**:295–301.
14. Reppert SM, Godson C, Mahle CD et al. Molecular characterization of a second melatonin receptor expressed in human retina and brain: the Mel1b melatonin receptor. Proc Natl Acad Sci U S A 1995; **92**:8734–8738.
15. Dubocovich ML, Yun K, Al-Ghoul WM et al. Selective MT2 melatonin receptor antagonists block melatonin-mediated phase advances of circadian rhythms. FASEB J 1998; **12**:1211–1220.
16. Hunt AE, Al-Ghoul WM, Gillette MU et al. Activation of MT(2) melatonin receptors in rat suprachiasmatic nucleus phase advances the circadian clock. Am J Physiol Cell Physiol 2001; **280**:C110–C118.
17. Drew JE, Barrett P, Mercer JG et al. Localization of the melatonin-related receptor in the rodent brain and peripheral tissues. J Neuroendocrinol 2001; **13**:453–458.
18. Savaskan E, Wirz-Justice A, Olivieri G et al. Distribution of melatonin MT1 receptor immunoreactivity in human retina. J Histochem Cytochem 2002; **50**:519–526.
19. Savaskan E, Ayoub MA, Ravid R et al. Reduced hippocampal MT2 melatonin receptor expression in Alzheimer's disease. J Pineal Res 2005; **38**:10–16.
20. Angeloni D, Longhi R, Fraschini F. Production and characterization of antibodies directed against the human melatonin receptors Mel-1a (mt1) and Mel-1b (MT2). Eur J Histochem 2000; **44**:199–204.
21. Nonno R, Lucini V, Pannacci M et al. Pharmacological characterization of the human melatonin Mel1a receptor following stable transfection into NIH3T3 cells. Br J Pharmacol 1998; **124**:485–492.
22. Nonno R, Pannacci M, Lucini V et al. Ligand efficacy and potency at recombinant human MT2 melatonin receptors:

evidence for agonist activity of some mt1-antagonists. Br J Pharmacol 1999; **127**:1288–1294.
23. Lacoste B, Riad M, Descarries L. Immunocytochemical evidence for the existence of substance P receptor (NK1) in serotonin neurons of rat and mouse dorsal raphe nucleus. Eur J Neurosci 2006; **23**:2947–2958.
24. Lacoste B, Riad M, Ratte MO et al. Trafficking of neurokinin-1 receptors in serotonin neurons is controlled by substance P within the rat dorsal raphe nucleus. Eur J Neurosci 2009; **29**:2303–2314.
25. Berube-Carriere N, Guay G, Fortin GM et al. Ultrastructural characterization of the mesostriatal dopamine innervation in mice, including two mouse lines of conditional VGLUT2 knockout in dopamine neurons. Eur J Neurosci 2012; **35**:527–538.
26. Aika Y, Ren JQ, Kosaka K et al. Quantitative analysis of GABA-like-immunoreactive and parvalbumin-containing neurons in the CA1 region of the rat hippocampus using a stereological method, the disector. Exp Brain Res 1994; **99**:267–276.
27. Dubocovich ML, Delagrange P, Krause DN et al. International Union of Basic and Clinical Pharmacology. LXXV. Nomenclature, classification, and pharmacology of G protein-coupled melatonin receptors. Pharmacol Rev 2010; **62**:343–380.
28. Vanecek J. Melatonin binding sites. J Neurochem 1988; **51**:1436–1440.
29. Perreau-Lenz S, Kalsbeek A, Garidou ML et al. Suprachiasmatic control of melatonin synthesis in rats: inhibitory and stimulatory mechanisms. Eur J Neurosci 2003; **17**:221–228.
30. Dubocovich ML, Rivera-Bermudez MA, Gerdin MJ et al. Molecular pharmacology, regulation and function of mammalian melatonin receptors. Front Biosci 2003; **8**:d1093–d1108.
31. Laitinen JT, Saavedra JM. Characterization of melatonin receptors in the rat suprachiasmatic nuclei: modulation of affinity with cations and guanine nucleotides. Endocrinology 1990; **126**:2110–2115.
32. Williams LM, Morgan PJ. Demonstration of melatonin-binding sites on the pars tuberalis of the rat. J Endocrinol 1988; **119**:R1–R3.
33. Morgan PJ, Williams LM, Davidson G et al. Melatonin receptors on ovine pars tuberalis: characterization and autoradiographicai localization. J Neuroendocrinol 1989; **1**:1–4.
34. Wu YH, Zhou JN, Balesar R et al. Distribution of MT1 melatonin receptor immunoreactivity in the human hypothalamus and pituitary gland: colocalization of MT1 with vasopressin, oxytocin, and corticotropin-releasing hormone. J Comp Neurol 2006; **499**:897–910.
35. Gauer F, Masson-Pevet M, Pevet P. Melatonin receptor density is regulated in rat pars tuberalis and suprachiasmatic nuclei by melatonin itself. Brain Res 1993; **602**:153–156.
36. Gauer F, Masson-Pevet M, Skene DJ et al. Daily rhythms of melatonin binding sites in the rat pars tuberalis and suprachiasmatic nuclei; evidence for a regulation of melatonin receptors by melatonin itself. Neuroendocrinology 1993; **57**:120–126.
37. Weaver D, Rivkees S, Reppert S. Localization and characterization of melatonin receptors in rodent brain by in vitro autoradiography. J Neurosci 1989; **9**:2581–2590.
38. Williams LM. Melatonin-binding sites in the rat brain and pituitary mapped by in-vitro autoradiography. J Mol Endocrinol 1989; **3**:71–75.
39. Laudon M, Nir I, Zisapel N. Melatonin receptors in discrete brain areas of the male rat. Impact of aging on density and on circadian rhythmicity. Neuroendocrinology 1988; **48**:577–583.
40. Williams LM, Hannah LT, Hastings MH et al. Melatonin receptors in the rat brain and pituitary. J Pineal Res 1995; **19**:173–177.
41. Uz T, Arslan AD, Kurtuncu M et al. The regional and cellular expression profile of the melatonin receptor MT1 in the central dopaminergic system. Brain Res Mol Brain Res 2005; **136**:45–53.
42. Ahn S-K, Khalmuratova R, Hah Y-S et al. Immunohistochemical and biomolecular identification of melatonin 1a and 1b receptors in rat vestibular nuclei. Auris Nasus Larynx 2012; **39**:479–483.
43. Poirel VJ, Masson-Pevet M, Pevet P et al. MT1 melatonin receptor mRNA expression exhibits a circadian variation in the rat suprachiasmatic nuclei. Brain Res 2002; **946**:64–71.
44. Mazzucchelli C, Pannacci M, Nonno R et al. The melatonin receptor in the human brain: cloning experiments and distribution studies. Brain Res Mol Brain Res 1996; **39**:117–126.
45. Musshoff U, Riewenherm D, Berger E et al. Melatonin receptors in rat hippocampus: molecular and functional investigations. Hippocampus 2002; **12**:165–173.
46. Stankov B, Cozzi B, Lucini V et al. Characterization and mapping of melatonin receptors in the brain of three mammalian species: rabbit, horse and sheep. A comparative in vitro binding study. Neuroendocrinology 1991; **53**:214–221.
47. Reiter R, Tan D, Manchester L et al. Medical implications of melatonin: receptor-mediated and receptor-independent actions. Adv Med Sci 2007; **52**:11–28.
48. Comai S, Ochoa-Sanchez R, Gobbi G. Sleep-wake characterization of double MT(1)/MT(2) receptor knockout mice and comparison with MT(1) and MT(2) receptor knockout mice. Behav Brain Res 2013; **243**:231–238.
49. Clement O, Sapin E, Libourel PA et al. The lateral hypothalamic area controls paradoxical (REM) sleep by means of descending projections to brainstem GABAergic neurons. J Neurosci 2012; **32**:16763–16774.
50. Hepp K, Henn V. Spatio-temporal recoding of rapid eye movement signals in the monkey paramedian pontine reticular formation (PPRF). Exp Brain Res 1983; **52**:105–120.
51. Lindroos O, Veilahti J, Leinonen L et al. Characterization of melatonin binding to the anteroventral and anterodorsal thalamic nuclei of the rat. Eur J Pharmacol 1993; **250**:161–163.
52. Dominguez-Lopez S, Howell R, Gobbi G. Characterization of serotonin neurotransmission in knockout mice: implications for major depression. Rev Neurosci 2012; **23**:429–443.
53. Comai S, Ochoa-Sanchez R, Dominguez-Lopez S et al. Melancholic-like behaviors and circadian neurobiological abnormalities in melatonin MT1 receptor knockout mice. Int J Neuropsychopharmacol 2015; **18**:1–10.
54. Dominguez-Lopez S, Mahar I, Bambico FR et al. Short-term effects of melatonin and pinealectomy on serotonergic neuronal activity across the light-dark cycle. J Psychopharmacol 2012; **26**:830–844.
55. Malpaux B, Daveau A, Maurice-Mandon F et al. Evidence that melatonin acts in the premammillary hypothalamic area to control reproduction in the ewe: presence of binding sites and stimulation of luteinizing hormone secretion by in situ microimplant delivery. Endocrinology 1998; **139**:1508–1516.

56. Silman R. Melatonin and the human gonadotrophin-releasing hormone pulse generator. J Endocrinol 1991; **128**:7–11.
57. Olcese J, Lozier S, Paradise C. Melatonin and the circadian timing of human parturition. Reprod Sci 2013; **20**: 168–174.
58. Savaskan E, Olivieri G, Meier F et al. Increased melatonin 1a-receptor immunoreactivity in the hippocampus of Alzheimer's disease patients. J Pineal Res 2002; **32**:59–62.
59. Brunner P, Sozer-Topcular N, Jockers R et al. Pineal and cortical melatonin receptors MT1 and MT2 are decreased in Alzheimer's disease. Eur J Histochem 2006; **50**:311–316.
60. Dominguez-Lopez S, Howell RD, Lopez-Canul MG et al. Electrophysiological characterization of dopamine neuronal activity in the ventral tegmental area across the light-dark cycle. Synapse 2014; **68**:454–467.
61. Sircar R. Effect of melatonin on cocaine-induced behavioral sensitization. Brain Res 2000; **857**:295–299.
62. Exposito I, Mora F, Zisapel N et al. The modulatory effect of melatonin on the dopamine-glutamate interaction in the anterior hypothalamus during ageing. NeuroReport 1995; **6**:2399–2403.
63. Adi N, Mash DC, Ali Y et al. Melatonin MT1 and MT2 receptor expression in Parkinson's disease. Med Sci Monit 2010; **16**:BR61–BR67.
64. Sumaya IC, Byers DM, Irwin LN et al. Circadian-dependent effect of melatonin on dopaminergic D2 antagonist-induced hypokinesia and agonist-induced stereotypies in rats. Pharmacol Biochem Behav 2004; **78**:727–733.
65. Pazo JH. Effects of melatonin on spontaneous and evoked neuronal activity in the mesencephalic reticular formation. Brain Res Bull 1979; **4**:725–730.
66. Castillo Romero JL, Vives Montero F, Acuna Castroviejo D. Paradoxical effects of melatonin on spontaneous neuronal activity in the striatum of sham-operated and pinealectomized rats. J Pineal Res 1992; **12**:149–154.
67. Naranjo-Rodriguez EB, Prieto-Gomez B, Reyes-Vazquez C. Melatonin modifies the spontaneous multiunit activity recorded in several brain nuclei of freely behaving rats. Brain Res Bull 1991; **27**:595–600.
68. Mason R, Brooks A. The electrophysiological effects of melatonin and a putative melatonin antagonist (*N*-acetyltryptamine) on rat suprachiasmatic neurones in vitro. Neurosci Lett 1988; **95**:296–301.
69. Ambriz-Tututi M, Rocha-Gonzalez HI, Cruz SL et al. Melatonin: a hormone that modulates pain. Life Sci 2009; **84**:489–498.
70. Lopez-Canul M, Palazzo E, Dominguez-Lopez S et al. Selective melatonin MT2 receptor ligands relieve neuropathic pain through modulation of brainstem descending antinociceptive pathways. Pain 2015; **156**:305–317.
71. Hahm ET, Kim Y, Lee JJ et al. GABAergic synaptic response and its opioidergic modulation in periaqueductal gray neurons of rats with neuropathic pain. BMC Neurosci 2011; **12**:41.
72. Yadin E, Thomas E, Grishkat HL et al. The role of the lateral septum in anxiolysis. Physiol Behav 1993; **53**:1077–1083.
73. Karakas A, Coskun H, Kaya A et al. The effects of the intraamygdalar melatonin injections on the anxiety like behavior and the spatial memory performance in male Wistar rats. Behav Brain Res 2011; **222**:141–150.
74. Ochoa-Sanchez R, Rainer Q, Comai S et al. Anxiolytic effects of the melatonin MT(2) receptor partial agonist UCM765: comparison with melatonin and diazepam. Prog Neuropsychopharmacol Biol Psychiatry 2012; **39**:318–325.
75. Jin X, Von Gall C, Pieschl RL et al. Targeted disruption of the mouse Mel(1b) melatonin receptor. Mol Cell Biol 2003; **23**:1054–1060.
76. Paxinos G, Watson C. *The Rat Brain in Stereotaxic Coordinates: Compact*. 6th edn. Academic Press, London, 2009.